Article

Developmental Cell

Endoderm development requires centrioles to restrain p53-mediated apoptosis in the absence of ERK activity

Graphical abstract

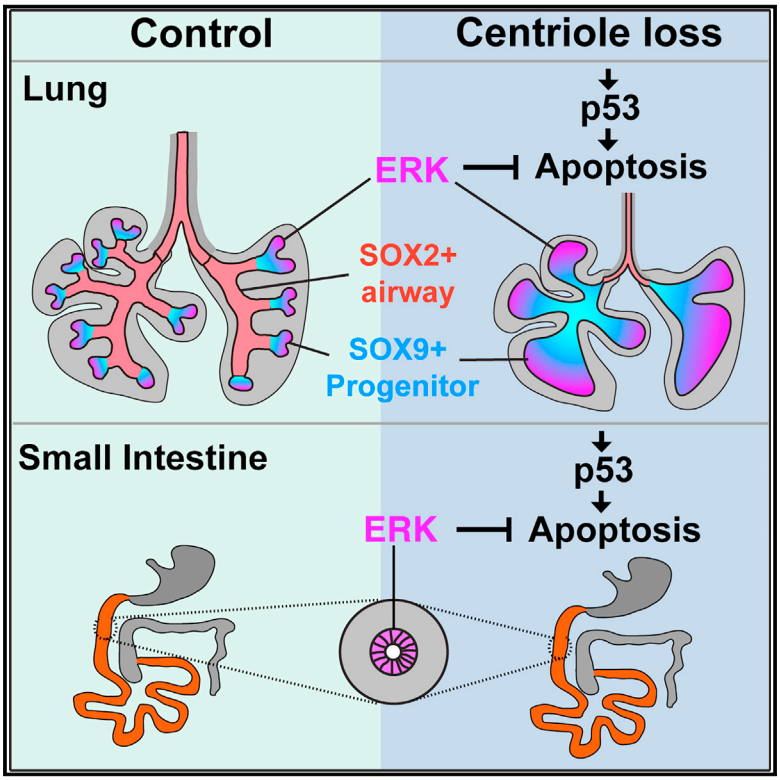

Highlights

- Endodermal centrioles are critical for lung branching but not for intestine development
- Centriole loss activates p53 to induce apoptosis in lung SOX2-expressing cells
- ERK activity throughout the small intestine protects it from p53-mediated apoptosis
- A gradient of ERK activity in the lungs shapes which cells die to block branching

Authors

Chang Xie, Shaun R. Abrams, Vicente Herranz-Pérez, Jose Manuel García-Verdugo, Jeremy F. Reiter

Correspondence

jeremy.reiter@ucsf.edu

In brief

Chang et al. show that endoderm centrioles are dispensable for intestinal development but essential for lung branching. Throughout both intestine and lungs, loss of centrioles activates p53, but the lack of centrioles induces apoptosis only in domains of low ERK signaling.

Xie et al., 2021, Developmental Cell *56*, 3334–3348
December 20, 2021
https://doi.org/10.1016/j.devcel.2021.11.020

CellPress

CellPress
OPEN ACCESS

Developmental Cell

Article

Endoderm development requires centrioles to restrain p53-mediated apoptosis in the absence of ERK activity

Chang Xie,[1] Shaun R. Abrams,[1] Vicente Herranz-Pérez,[2,3] Jose Manuel García-Verdugo,[2] and Jeremy F. Reiter[1,4,5,*]
[1]Department of Biochemistry and Biophysics, Cardiovascular Research Institute, University of California, San Francisco, San Francisco, CA, USA
[2]Cavanilles Institute of Biodiversity and Evolutionary Biology, University of Valencia, Valencia, Spain
[3]Predepartamental Unit of Medicine, Jaume I University, Castelló de la Plana, Spain
[4]Chan Zuckerberg Biohub, San Francisco, CA 94158, USA
[5]Lead contact
*Correspondence: jeremy.reiter@ucsf.edu
https://doi.org/10.1016/j.devcel.2021.11.020

SUMMARY

Centrioles comprise the heart of centrosomes, microtubule-organizing centers. To study the function of centrioles in lung and gut development, we genetically disrupted centrioles throughout the mouse endoderm. Surprisingly, removing centrioles from the endoderm did not disrupt intestinal growth or development but blocked lung branching. In the lung, acentriolar SOX2-expressing airway epithelial cells apoptosed. Loss of centrioles activated p53, and removing p53 restored survival of SOX2-expressing cells, lung branching, and mouse viability. To investigate how endodermal p53 activation specifically killed acentriolar SOX2-expressing cells, we assessed ERK, a prosurvival cue. ERK was active throughout the intestine and in the distal lung buds, correlating with tolerance to centriole loss. Pharmacologically inhibiting ERK activated apoptosis in acentriolar cells, revealing that ERK activity protects acentriolar cells from apoptosis. Therefore, centrioles are largely dispensable for endodermal growth and the spatial distribution of ERK activity in the endoderm shapes the developmental consequences of centriolar defects and p53 activation.

INTRODUCTION

Each centriole is comprised of nine triplet microtubules arranged in a cylinder. Two centrioles and the pericentriolar materials make up the centrosome, the principal microtubule-organizing center in mammalian cells. Centrioles are at the heart of the mitotic poles during cell division and, in their roles as basal bodies, act as the cilium's foundation.

Much like chromosomes, centrioles are duplicated once and only once per cell cycle. *Cenpj* encodes SAS-4, also called CPAP, a core component of centrioles essential for centriole duplication (Gönczy, 2012). Human mutations in *CENPJ* cause microcephaly, a defect in brain growth, or Seckel syndrome, a general growth deficit (Al-Dosari et al., 2010; Bond et al., 2005). Consistent with the critical functions of centrioles in development, mouse embryos without CENPJ die at mid-gastrulation (Bazzi and Anderson, 2014). Pharmacologically inhibiting another protein required for centriole duplication, PLK4, causes noncancer cells to undergo G1 arrest (Wong et al., 2015), suggesting that centrioles are broadly essential for mammalian cell division.

Loss of centrioles activates p53 (TP53), a tumor suppressor that interprets various cell stresses (Bazzi and Anderson, 2014; Kastenhuber and Lowe, 2017; Wong et al., 2015). One direct transcriptional target of p53 is p21 (CDKN1A), a cyclin-dependent kinase (CDK) inhibitor that induces cell-cycle arrest (el-Deiry et al., 1993; Harper et al., 1993). In cancer, p53 and p21 can be antagonized by activation of extracellular signal-regulated kinase (ERK) (Yang et al., 2017).

A diverse range of developmental syndromes are associated with activated p53, implicating increased p53 activity in the etiology of birth defects (Bowen and Attardi, 2019; Van Nostrand et al., 2014). In support of this possibility, activating mutations in p53 or attenuating a negative regulator of p53 causes developmental phenotypes in humans (Lessel et al., 2017; Toki et al., 2018). Moreover, deletion of p53 can partly or fully rescue defects in mouse genetic models of developmental syndromes (Bowen et al., 2019). For example, deletion of p53 reduces the increased cell death observed in *Cenpj* null embryos (Bazzi and Anderson, 2014).

The neural epithelium undergoes dramatic expansion during midgastrulation and is particularly dependent on CENPJ function (Bazzi and Anderson, 2014), suggesting that actively dividing cells are especially susceptible to centriole loss. Like the neural epithelium, the endodermal epithelium undergoes dramatic expansion during embryonic development (Zorn and Wells, 2009). We hypothesized that centrioles would, like for the neural epithelium,

CellPress
OPEN ACCESS

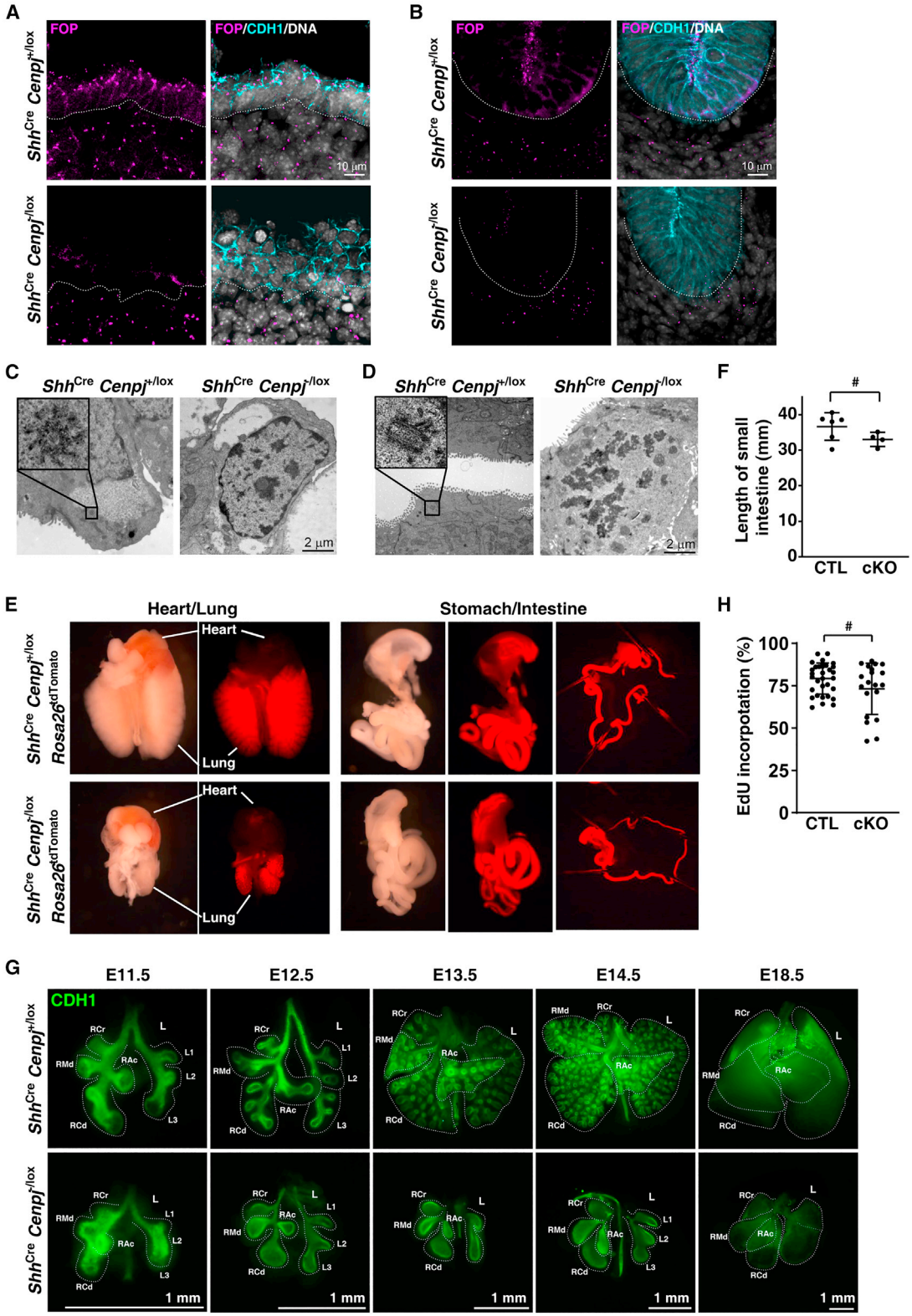

Figure 1. Endodermal centrioles are essential for lung branching, but not for intestinal development

(A and B) Immunostaining of E11.5 control (*Shh*^{Cre} *Cenpj*$^{+/lox}$) and *Cenpj* loss-of-function (*Shh*^{Cre} *Cenpj*$^{-/lox}$) lung (A) and small intestine (B) sections for centrioles (FOP, magenta), epithelium (CDH1, cyan), and nuclei (Hoechst, gray). Scale bars, 10 μm.

(legend continued on next page)

be critical for endodermal epithelial development and, consequently, the development of the alimentary tract and lungs.

To test this hypothesis, we removed *Cenpj* throughout the endoderm. Surprisingly, loss of centrioles had minimal effects on the growth and development of the small intestine. In contrast, in the lung, loss of centrioles severely attenuated lung branching. Within the developing acentriolar lungs, SOX9-expressing progenitors survived and expanded but failed to give rise to SOX2-expressing airway cells. We found that in the developing intestine, ERK activity is broadly active, but in the developing lung, ERK activity is restricted to the distal tip of lung buds where the SOX9-expressing cells reside. Pharmacological inhibition revealed that ERK is critical for the survival of SOX9-expressing lung progenitors and intestinal cells lacking centrioles. These results indicate that centrioles are differentially required for distinct endodermal lineages and that differential ERK activity underlies the differences in phenotypic consequences caused by loss of centrioles.

RESULTS

Epithelial centrioles are essential for lung branching but dispensable for intestinal development

To test whether centrioles are essential for the proliferation of quickly growing cells such as the endodermal epithelium, we used Shh^{Cre} to conditionally delete *Cenpj*, the ortholog of *C. elegans sas-4* throughout the endoderm. Centrioles were identified by staining for the centriolar protein FOP (FGFR1OP), and epithelia were identified by staining for E-cadherin (CDH1). Centrioles were present in mesenchymal and epithelial cells in control (Shh^{Cre} $Cenpj^{+/lox}$) lungs and intestines but absent specifically from the endodermal epithelia of mutant (Shh^{Cre} $Cenpj^{-/lox}$) lungs and intestines (Figures 1A and 1B), indicating that CENPJ is essential for centriole biogenesis in the endoderm.

To confirm that we had successfully removed centrioles from the endoderm, we used serial-section transmission electron microscopy (TEM). Control lung and intestinal epithelial cells contained centrioles, recognized by their characteristic 9-fold symmetry (Figures 1C and 1D). In contrast, Shh^{Cre} $Cenpj^{-/lox}$ lung and intestinal epithelial cells possessed no centrioles (Figures 1C, 1D, S1, and S2). Shh^{Cre} induced recombination of the tdTomato reporter throughout the endoderm (Figure 1E), suggesting that the endoderm of Shh^{Cre} $Cenpj^{-/lox}$ embryos is acentriolar.

At E16.5, the gross appearance and length of Shh^{Cre} $Cenpj^{-/lox}$ small intestines were indistinguishable from those of controls (Figures 1E and 1F). In marked contrast, Shh^{Cre} $Cenpj^{-/lox}$ lung development was dramatically perturbed. Thus, endodermal centrioles are essential for lung development but dispensable for intestine development.

During embryogenesis, the lung epithelium branches and ramifies into its surrounding mesenchyme (Metzger et al., 2008). Wholemount E11.5 lungs stained for CDH1 revealed that both control and mutant mouse embryos possessed four major lobes on the right side (right cranial [RCr], right middle [RMd], right accessory [RAc], and right caudal [RCd]) and three main secondary branches on the left lobe (L1-L3). At E12.5, the major lobes of mutant lungs had failed to branch (Figure 1G).

Lungs grow throughout embryogenesis. Measuring EdU incorporation revealed that cell-cycle engagement in the lung epithelium does not depend on centrioles and that Shh^{Cre} $Cenpj^{-/lox}$ lungs grow throughout all lung developmental stages until birth (Figure 1H). Mutant pups died at birth, attributable to disrupted lung development. Therefore, endodermal centrioles are not essential for proliferation but are critical for lung branching.

Development of lung SOX2-expressing cells depends on CENPJ

The embryonic lung epithelium comprises two main populations, the SOX2-expressing proximal airway epithelium cells (trachea, bronchi, and bronchioles) and SOX9-expressing progenitors at the distal bud tips. During the pseudoglandular stage (E12-E16.5 in mouse), the lung distal tip cells proliferate rapidly to give rise to both the repetitively branching outgrowths and the more proximal SOX2-expressing bronchiolar epithelium that form the conducting airways of the lung (Alanis et al., 2014; Rawlins et al., 2009).

To analyze cell differentiation during lung branching morphogenesis, we stained E12.5 to E15.5 wholemount lungs for SOX9 and SOX2. During control lung development, SOX9-expressing cells remained restricted to ramifying distal tips, and there was a concomitant increase in SOX2-expressing bronchioles (Figure 2A, upper panel). Shh^{Cre} $Cenpj^{-/lox}$ lungs developed major lobes, comparable with control lungs. However, in mutant lungs, SOX9-expressing cells expanded and, consistent with the absence of branching, were not constrained to distal tips (Figure 2A).

In addition to SOX9, distal epithelial cells express NKX2-1 (also known as TTF1) and SFTPC (Beers et al., 1992; Lazzaro et al., 1991). We examined their expression and found that Shh^{Cre} $Cenpj^{-/lox}$ lung epithelia expressed both (Figures S3A–S3C). These findings confirm that centrioles are not essential for the distal epithelial lung fate.

Early (E12.5) in lung development, mutant lungs contained fewer SOX2-expressing cells than control lungs, and mutant

(C and D) Transmission electron microscopy of E16.5 control (Shh^{Cre} $Cenpj^{+/lox}$) and *Cenpj* loss-of-function (Shh^{Cre} $Cenpj^{-/lox}$) lung (C) and small intestine (D) epithelium. Other images from these serially sectioned lung cells are included in Figures S1 and S2. No centrioles were detected in Shh^{Cre} $Cenpj^{-/lox}$ lung and intestinal epithelial cells. Scale bars, 2 μm.

(E) Gross appearance of the hearts, lungs and intestine from the control (Shh^{Cre} $Cenpj^{+/lox}$ $Rosa26^{tdTomato}$) and *Cenpj* loss-of-function (Shh^{Cre} $Cenpj^{-/lox}$ $Rosa26^{tdTomato}$) embryos at E16.5.

(F) Statistics of the length of control (CTL, Shh^{Cre} $Cenpj^{+/lox}$) and *Cenpj* loss-of-function (cKO, Shh^{Cre} $Cenpj^{-/lox}$) small intestine. # denotes no statistical significance, p = 0.1292, n = 5 for CTL, and n = 4 for cKO.

(G) Wholemount immunostaining of control (Shh^{Cre} $Cenpj^{+/lox}$) and *Cenpj* loss-of-function (Shh^{Cre} $Cenpj^{-/lox}$) lungs for CDH1 at E11.5, E12.5, E13.5, E14.5, and E18.5. Dashed lines outline the major lobes including right cranial (RCr), right middle (RMd), right accessory (RAc), right caudal (RCd), and left (L) lobes. Scale bars, 1 mm.

(H) Measurement of EdU incorporation into replicating DNA of E12.5 control (Shh^{Cre} $Cenpj^{+/lox}$) and Cenpj loss-of-function (Shh^{Cre} $Cenpj^{-/lox}$) lung epithelium. # denotes statistical insignificance, p = 0.1648. n = 9, 11, 16, and 8, respectively.

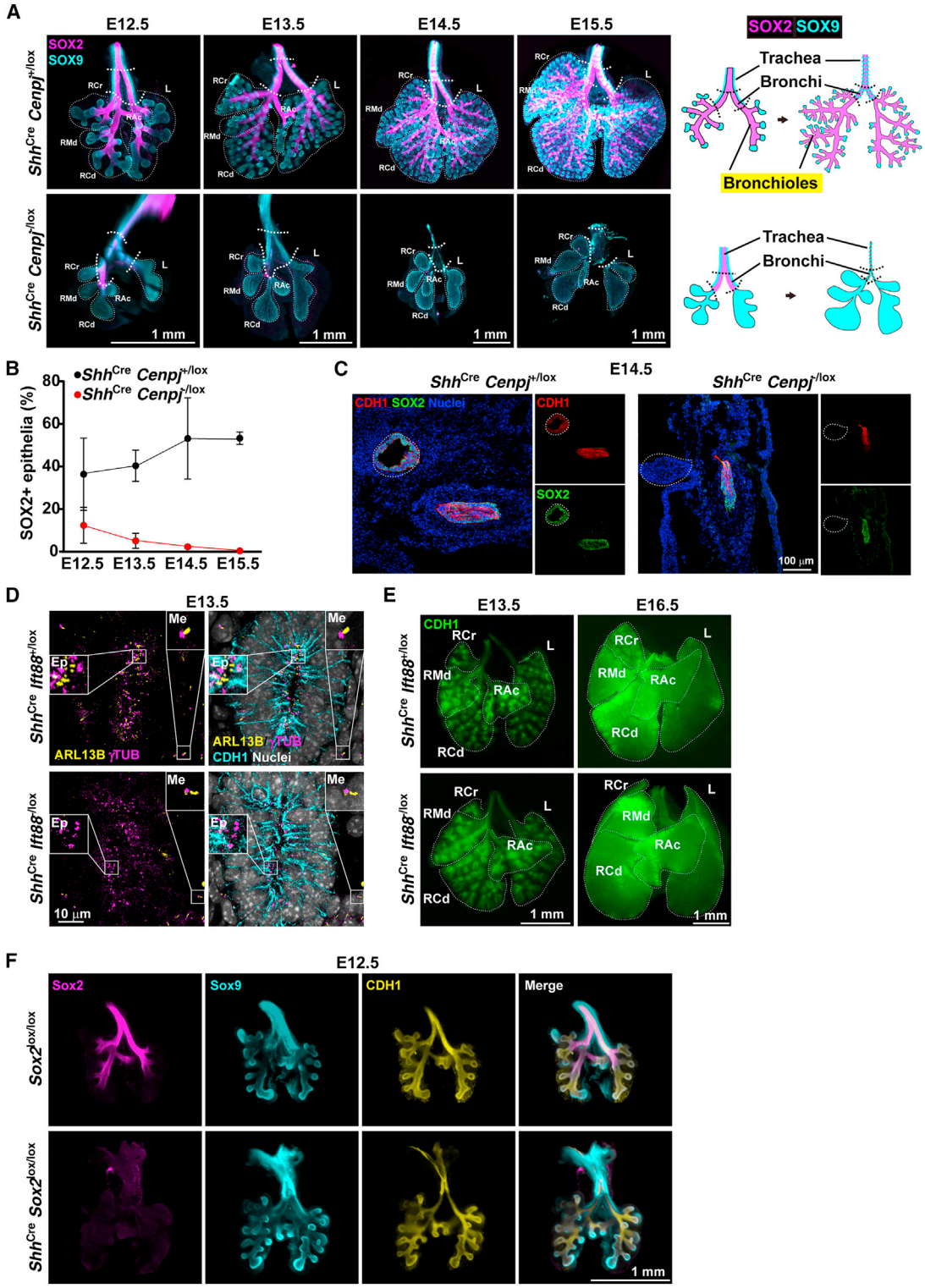

Figure 2. Centrioles are required for the development of SOX2-expressing lung epithelium

(A) Wholemount immunostaining of E12.5, E13.5, E14.5, and E15.5 control (*Shh*^{Cre} *Cenpj*$^{+/lox}$) and *Cenpj* loss-of-function (*Shh*^{Cre} *Cenpj*$^{-/lox}$) lungs for SOX2 (magenta) and SOX9 (cyan). The schematic (right) illustrates the expression of SOX2 in the trachea, bronchi, and bronchioles and of SOX9 in the tracheal rings and distal tip progenitors of lung. Scale bars, 1 mm.

(B) Quantification of the percentage of epithelium expressing SOX2. Maximum projection images of wholemount staining from (A) were analyzed (n = 3).

(legend continued on next page)

lungs were devoid of SOX2-expressing cells by E14.5 (Figure 2A). Measurement of the percentage of SOX2-expressing cells in the epithelium showed a gradual reduction from E12.5 and total loss of SOX2-expressing cells by E14.5 (Figure 2B). The absence of CDH1 at the trachea/bronchi confirmed the loss of SOX2-expressing epithelium by E14.5 (Figure 2C). Thus, CENPJ is essential for distal SOX9-expressing progenitors to give rise to SOX2-expressing bronchiolar epithelial cells.

Endodermal cilia are dispensable for lung branching morphogenesis

One critical function of centrioles is to support the formation of the primary cilium, a cellular antenna important for lung development (Abdelhamed et al., 2015; Dyson et al., 2017). Primary cilia, identified by staining for the ciliary component ARL13B, were associated with centrosomes, identified by staining for γTubulin (γTUB) (Figure 2D). Both lung mesenchymal and epithelial cells possessed cilia during development (Figure 2D).

To investigate whether the role of centrioles in lung branching is mediated through ciliogenesis, we investigated whether lung branching depends on cilia. We removed IFT88, a component of intraflagellar transport machinery essential for ciliogenesis and ciliary maintenance (Davenport et al., 2007) throughout the endoderm by generating *Shh*^{Cre} *Ift88*$^{-/lox}$ embryos. As expected, *Shh*^{Cre} *Ift88*$^{-/lox}$ lungs possessed cilia on their mesenchymal cells but not on their epithelial cells, indicating that removing IFT88 from the endoderm abrogates ciliogenesis in the developing lung epithelium (Figure 2D).

Wholemount staining of E13.5 and E16.5 control and *Shh*^{Cre} *Ift88*$^{-/lox}$ lungs revealed that branching was indistinguishable (Figure 2E). Impressively, *Shh*^{Cre} *Ift88*$^{-/lox}$ mice were viable through adulthood, indicating that endodermal cilia are not essential for lung function. Interestingly, limb digits 4 and 5 of *Shh*^{Cre} *Ift88*$^{-/lox}$ mice were atrophied (Figures S4B and S4D). As digits 4 and 5 are generated from the domain of *Shh* expression, the zone of polarizing activity (ZPA) (Ahn and Joyner, 2004), cilia transduce Hedgehog signals within the ZPA. As endodermal cilia are dispensable for lung branching, we conclude that centrioles function in lung branching independent of their role in ciliogenesis.

SOX2 is dispensable for lung branching morphogenesis

Deletion of SOX2 in part of the endoderm disrupts lung development (Que et al., 2007). Therefore, we hypothesized that the abrogation of SOX2 expression in *Shh*^{Cre} *Cenpj*$^{-/lox}$ lungs blocked branching in acentriolar lungs. To test this hypothesis, we removed SOX2 throughout the endoderm by generating *Shh*^{Cre} *Sox2*$^{lox/lox}$ embryos.

We stained wholemount lungs from *Shh*^{Cre} *Sox2*$^{lox/lox}$ and littermate control embryos for SOX2, SOX9, and CDH1. As expected, SOX2 was expressed in the developing trachea, bronchi, and bronchioles of control lungs and was absent from *Shh*^{Cre} *Sox2*$^{lox/lox}$ lungs at E12.5 (Figure 2F). CDH1 and SOX9 staining revealed that lung branching was unaffected in *Shh*^{Cre} *Sox2*$^{lox/lox}$ lungs (Figure 2F). Thus, compromised expression of SOX2 does not recapitulate the lung branching defect caused by loss of CENPJ.

In addition to SOX2, bronchiolar epithelial cells express the transcription factor p73 (Marshall et al., 2016; Nemajerova et al., 2016). As expected, p73 and SOX2 were coexpressed in the bronchiolar epithelium of control E16.5 lungs (Figures S3E and S3F). In contrast, *Shh*^{Cre} *Cenpj*$^{-/lox}$ lungs were devoid of p73-expressing cells (Figures S3E and S3F). These results confirm that CENPJ is required for bronchiolar epithelial formation and raise the possibility that SOX2- and p73-expressing cells critically depend on centrioles.

Loss of CENPJ in the endoderm activates p53 and apoptosis

As neither the absence of cilia nor loss of SOX2 function could account for how centriole loss disrupts lung branching, we analyzed the transcriptomes of control and *Shh*^{Cre} *Cenpj*$^{-/lox}$ lungs using RNA-seq. To identify gene expression changes caused by loss of centrioles and not cilia, we compared RNA-seq transcriptomes of control (*Shh*^{Cre} *Cenpj*$^{+/lox}$), cilia-disrupted (*Shh*^{Cre} *Ift88*$^{-/lox}$), and centriole-disrupted (*Shh*^{Cre} *Cenpj*$^{-/lox}$) lungs at E11.5, a time point prior to the emergence of a branching defect in acentriolar lungs (Table S1).

Genes differentially expressed in acentriolar lungs compared with control and cilia-disrupted lungs (in which branching is unaffected) are presented in a heatmap (Figure 3A). The fold changes and adjusted p values (FDR) of genes differentially expressed in acentriolar lungs are presented as a volcano plot (Figure 3B). *Sox2* was the most downregulated protein-coding gene in *Shh*^{Cre} *Cenpj*$^{-/lox}$ lungs, providing an orthogonal confirmation of the decrease of SOX2-expressing cells. Target genes of the WNT pathway (e.g., *Axin2* and *Bmp4*) and FGF pathway (e.g., *Etv4* and *Etv5*) were not significantly changed, suggesting that these developmental pathways were unaffected in *Cenpj* mutant lungs (Figure 3B).

The genes most significantly upregulated in *Shh*^{Cre} *Cenpj*$^{-/lox}$ lungs included p53 target genes such as *p21* (*Cdkn1a*), *Eda2r*, *Tap*, *Ccng1*, *Zfp365*, *Ddit4l*, *Dcxr*, and *Klhdc7a* (Allen et al., 2014; Bowen et al., 2019; Brosh et al., 2010; Forsberg et al., 2013; Turrell et al., 2017; Zhu et al., 1999) (Figure 3B). We confirmed the differential expression of *p21*, *Eda2r*, *Ccng1*, and *Sox2* by qRT-PCR (Figure 3C), further suggesting that p53

(C) Immunostaining of CDH1 in frozen sections of E14.5 control (*Shh*^{Cre} *Cenpj*$^{+/lox}$) and *Cenpj* loss-of-function (*Shh*^{Cre} *Cenpj*$^{-/lox}$) lungs. Images are of sections through the trachea and esophagus. White dashed lines outline the trachea. Scale bars, 100 μm.
(D) Immunostaining of E13.5 control (*Shh*^{Cre} *Ift88*$^{+/lox}$) and *Ift88* loss-of-function (*Shh*^{Cre} *Ift88*$^{-/lox}$) lung sections for cilia (ARL13B, yellow), centrosomes (γTubulin, γTUB, magenta), epithelium (CDH1, cyan), and nuclei (Hoechst, gray). Scale bars, 10 μm.
(E) Wholemount immunostaining of E13.5 and E16.5 control (*Shh*^{Cre} *Ift88*$^{+/lox}$) and *Ift88* loss-of-function (*Shh*^{Cre} *Ift88*$^{-/lox}$) lungs for CDH1. Dashed lines outline the major lobes. Scale bars, 1 mm.
(F) Wholemount immunostaining of E12.5 control (*Sox2*$^{lox/lox}$) and *Sox2* loss-of-function (*Shh*^{Cre} *Sox2*$^{lox/lox}$) lungs for SOX2 (magenta), SOX9 (cyan), and epithelium (CDH1, yellow). Scale bars, 1 mm.
See also Figures S3 and S4.

CellPress
OPEN ACCESS

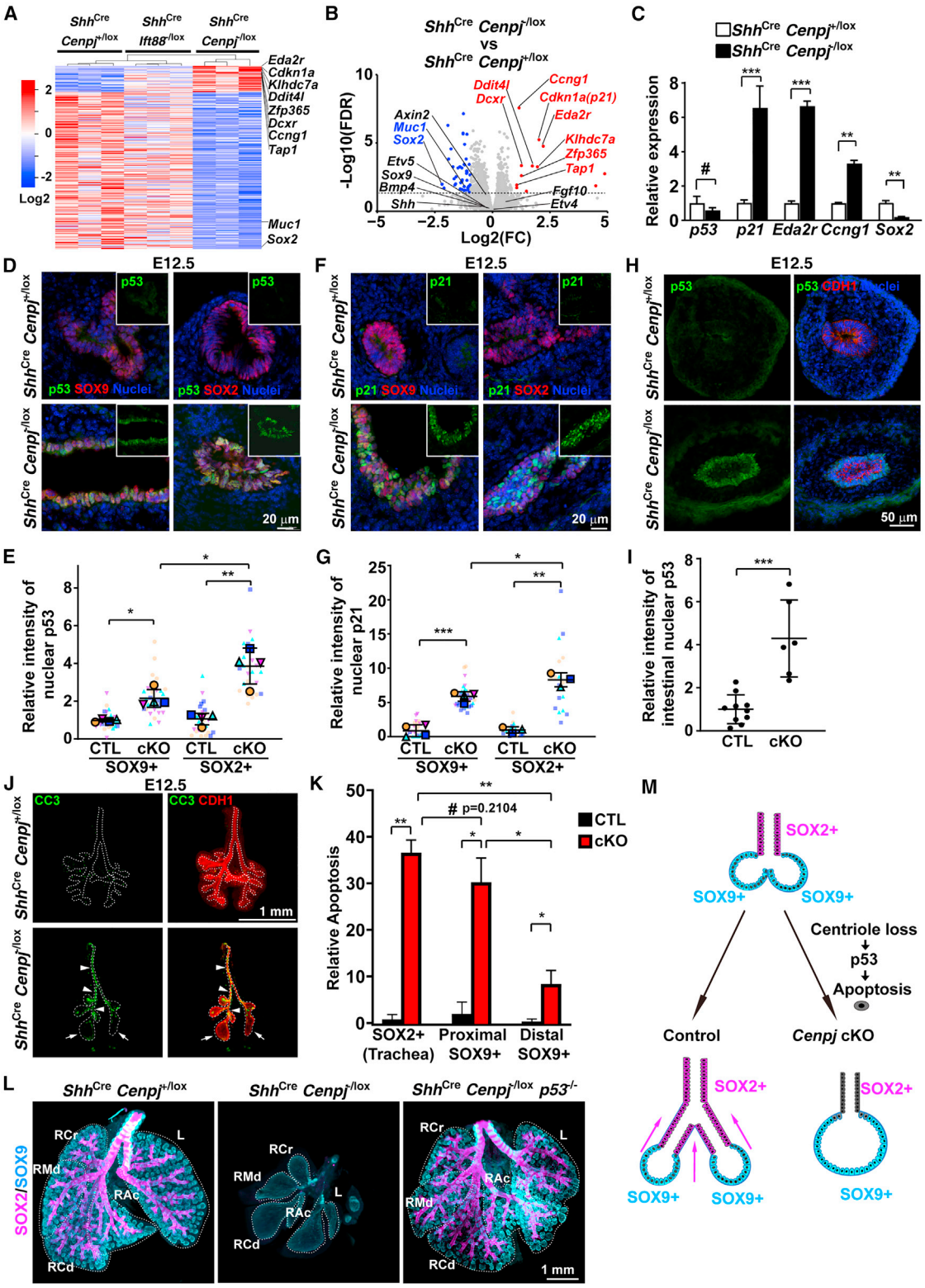

Figure 3. Centriole loss in endoderm activates p53-dependent apoptosis

(A) Heatmap of E11.5 control (*Shh*^{Cre} *Cenpj*$^{+/lox}$), *Ift88* loss-of-function (*Shh*^{Cre} *Ift88*$^{-/lox}$), and *Cenpj* loss-of-function (*Shh*^{Cre} *Cenpj*$^{-/lox}$) lung RNA-seq. Some significant differentially expressed genes from Cenpj loss-of-function (*Shh*^{Cre} *Cenpj*$^{-/lox}$) lung against control (*Shh*^{Cre} *Cenpj*$^{+/lox}$), *Ift88* loss-of-function (*Shh*^{Cre} *Ift88*$^{-/lox}$) lungs were listed in heatmap. *Cdkn1a* (*p21*) and several other p53-induced genes are specifically upregulated upon loss of CENPJ.

(legend continued on next page)

is active in *Shh*^{Cre} *Cenpj*$^{-/lox}$ lungs. The expression of the gene encoding p53, *Trp53*, was unaffected in acentriolar lungs, consistent with p53 activity being principally controlled post-transcriptionally.

To determine whether p53 was activated in the endoderm, we stained control and *Shh*^{Cre} *Cenpj*$^{-/lox}$ lungs and small intestine for p53. p53 was nearly undetectable in control lungs and small intestine and dramatically increased in nuclei of *Shh*^{Cre} *Cenpj*$^{-/lox}$ lung epithelial cells (Figures 3D and 3E). Similarly, the established p53 target, p21, was also upregulated in the nuclei of *Shh*^{Cre} *Cenpj*$^{-/lox}$ lungs (Figures 3F and 3G).

In parallel with the analysis of lung transcriptomes, we conducted RNA-seq analyses of control (*Shh*^{Cre} *Cenpj*$^{+/lox}$), cilia-disrupted (*Shh*^{Cre} *Ift88*$^{-/lox}$), and centriole-disrupted (*Shh*^{Cre} *Cenpj*$^{-/lox}$) E11.5 small intestines. Compared with the lungs, loss of CENPJ perturbed gene expression more modestly in the intestine (Table S2). Despite the less significant effect of loss of centrioles on intestinal gene expression, we examined whether p53 was activated in the acentriolar intestinal epithelium as it was in the lung epithelium. Nuclear p53 was present at negligible levels in control E13.5 intestines and upregulated in the intestinal epithelium of *Shh*^{Cre} *Cenpj*$^{-/lox}$ embryos (Figures 3H and 3I). Thus, despite the dramatically different effects on lung and intestinal development, loss of centrioles activates p53 in both tissues.

p53 activation can induce apoptosis (Aubrey et al., 2018). To begin to assess whether p53-triggered apoptosis could account for the loss of SOX2-expressing cells and branching in *Shh*^{Cre} *Cenpj*$^{-/lox}$ lungs, we assessed the presence of cleaved Caspase3 (CC3). Cleaved Caspase3 was almost undetectable in control lungs and dramatically upregulated specifically in the epithelium of *Shh*^{Cre} *Cenpj*$^{-/lox}$ lungs (Figures 3J and 3K). Quantitating the spatial distribution of apoptotic cells revealed dramatically elevated levels in the proximal *Shh*^{Cre} *Cenpj*$^{-/lox}$ lungs and more mild increases in the distal lungs (Figures 3J and 3K). The high levels of apoptosis, therefore, correlate with the presence of SOX2-expressing cells in the developing trachea and bronchi (Figures 2A and 2B). Therefore, we hypothesized that loss of centrioles induced p53-mediated apoptosis in the proximal regions of the developing lung to disrupt branching.

Removing p53 restores branching to acentriolar lungs

To test whether p53 activation underlies the lung branching defect, we generated *Shh*^{Cre} *Cenpj*$^{-/lox}$ p53$^{-/-}$ lungs. Mice lacking p53 are viable and did not display discernible differences in lung morphology, indicating that p53 is not required for lung development (data not included). We stained wholemount lungs from E15.5 control, *Shh*^{Cre} *Cenpj*$^{-/lox}$, and *Shh*^{Cre} *Cenpj*$^{-/lox}$ p53$^{-/-}$ embryos for SOX2 and SOX9. As observed previously, loss of CENPJ disrupted lung branching and led to loss of SOX2-expressing epithelial cells. In stark contrast, *Shh*^{Cre} *Cenpj*$^{-/lox}$ p53$^{-/-}$ lungs displayed lung branching indistinguishable from those of control mice (Figure 3L). In addition, removal of p53 restored SOX2-expressing airway cells to *Shh*^{Cre} *Cenpj*$^{-/lox}$ lungs. Impressively, *Shh*^{Cre} *Cenpj*$^{-/lox}$ *p53*$^{-/lox}$ mice were viable through adulthood (Figures S4A and S4C). As removing p53 entirely rescued lung development in *Shh*^{Cre} *Cenpj*$^{-/lox}$ p53$^{-/-}$ mice, we conclude that, in the absence of p53, centrioles are dispensable throughout the endoderm for lung development and animal viability.

Interestingly, *Shh*^{Cre} *Cenpj*$^{-/lox}$ *p53*$^{-/lox}$ mice exhibited atrophic digits 4 and 5, similar to those of *Shh*^{Cre} *Ift88*$^{-/lox}$ mice (Figures S4A–S4D). The finding that both centrioles and cilia are essential in limb bud cells to generate digits, regardless of whether p53 is active, is consistent with an essential role for centrioles in generating the primary cilia required to interpret the Hedgehog cues essential for digit development (Huangfu and Anderson, 2005).

The finding that inhibiting p53 restores lung branching to acentriolar lungs reveals that p53 activation disrupts branching. Lungs branch as the distal fields of SOX9-expressing progenitors are bifurcated and as proximal field progenitors differentiate into SOX2-expressing airway epithelium (Alanis et al., 2014; Rawlins et al., 2009). Centriole loss activates p53 to induce apoptosis preferentially depleting the SOX2-expressing cells. We propose that the loss of these SOX2-expressing cells in the distal airway prevents bifurcation of the progenitor field and thereby disrupts branching (schematized in Figure 3M). These findings raise the interesting question of why centrioles are essential for SOX2-expressing lung cells but dispensable for SOX9-expressing lung cells and intestinal epithelial cells, despite the shared activation of p53.

(B) Volcano plot comparing $\log_2$ fold change of normalized RNA-seq reads for E11.5 *Cenpj* loss-of-function (*Shh*^{Cre} *Cenpj*$^{-/lox}$) with control (*Shh*^{Cre} *Cenpj*$^{+/lox}$) lungs. The dashed line denotes the p = 0.05 cutoff. Selected genes upregulated ≥2 fold were indicated in red, and selected genes downregulated ≥2 fold were indicated in blue (FDR < 0.05).

(C) qRT-PCR measurement of *Cdkn1a* (p21), *Ccng1*, *Eda2r*, and *Sox2* expression in E13.5 control (*Shh*^{Cre} *Cenpj*$^{+/lox}$) and *Cenpj* loss-of-function (*Shh*^{Cre} *Cenpj*$^{-/lox}$) lungs. *Sox2* was downregulated and *Cdkn1a* (p21), *Ccng1*, and *Eda2r* upregulated upon loss of CENPJ. n = 4, 4, 4, 4, 3, and 3, respectively, for the control groups; n = 3, 4, 4, 4, 3, and 3, respectively, for *Cenpj* loss-of-function groups.

(D and E) Staining (D) and quantification (E) of p53 in E12.5 control (CTL, *Shh*^{Cre} *Cenpj*$^{+/lox}$) and *Cenpj* loss-of-function (cKO, *Shh*^{Cre} *Cenpj*$^{-/lox}$) lung cryosections. Scale bars, 20 μm. Four independent replicates were analyzed for statistics.

(F and G) Staining (F) and quantification (G) of p21 in E12.5 control (*Shh*^{Cre} *Cenpj*$^{+/lox}$) and *Cenpj* loss-of-function (*Shh*^{Cre} *Cenpj*$^{-/lox}$) lung cryosections. Scale bars, 20 μm. Four and three independent replicates for SOX9+ and SOX2+, respectively, were analyzed for statistics.

(H and I) Staining (H) and quantification (I) of p53 in E12.5 control (*Shh*^{Cre} *Cenpj*$^{+/lox}$) and *Cenpj* loss-of-function (*Shh*^{Cre} *Cenpj*$^{-/lox}$) small intestine cryosections. Scale bars, 50 μm. n = 10 and 6 for CTL and cKO, respectively.

(J and K) Staining (J) and quantification (K) of cleaved Caspase3 (CC3, green) in E12.5 control (*Shh*^{Cre} *Cenpj*$^{+/lox}$) and *Cenpj* loss-of-function (*Shh*^{Cre} *Cenpj*$^{-/lox}$) lungs. Epithelia (CDH1, red) are outlined by the dashed line. Arrows indicate the distal region of *Cenpj* loss-of-function lung, and arrowheads indicate the proximal part. Scale bars, 1 mm. n = 3.

(L) Wholemount immunostaining of E15.5 control (*Shh*^{Cre} *Cenpj*$^{+/lox}$), *Cenpj* loss-of-function (*Shh*^{Cre} *Cenpj*$^{-/lox}$), *Cenpj* and *p53* combined loss-of-function (*Shh*^{Cre} *Cenpj*$^{-/lox}$ *p53*$^{-/-}$) lungs for SOX2 (magenta) and SOX9 (cyan). Scale bars, 1 mm.

(M) A schematic showing the proposed mechanism by which centrioles participate in lung branching. In the absence of centrioles, proximal SOX2-expressing, but not distal SOX9-expressing, cells activate p53 to trigger apoptosis.

See also Figure S4 and Tables S1 and S2.

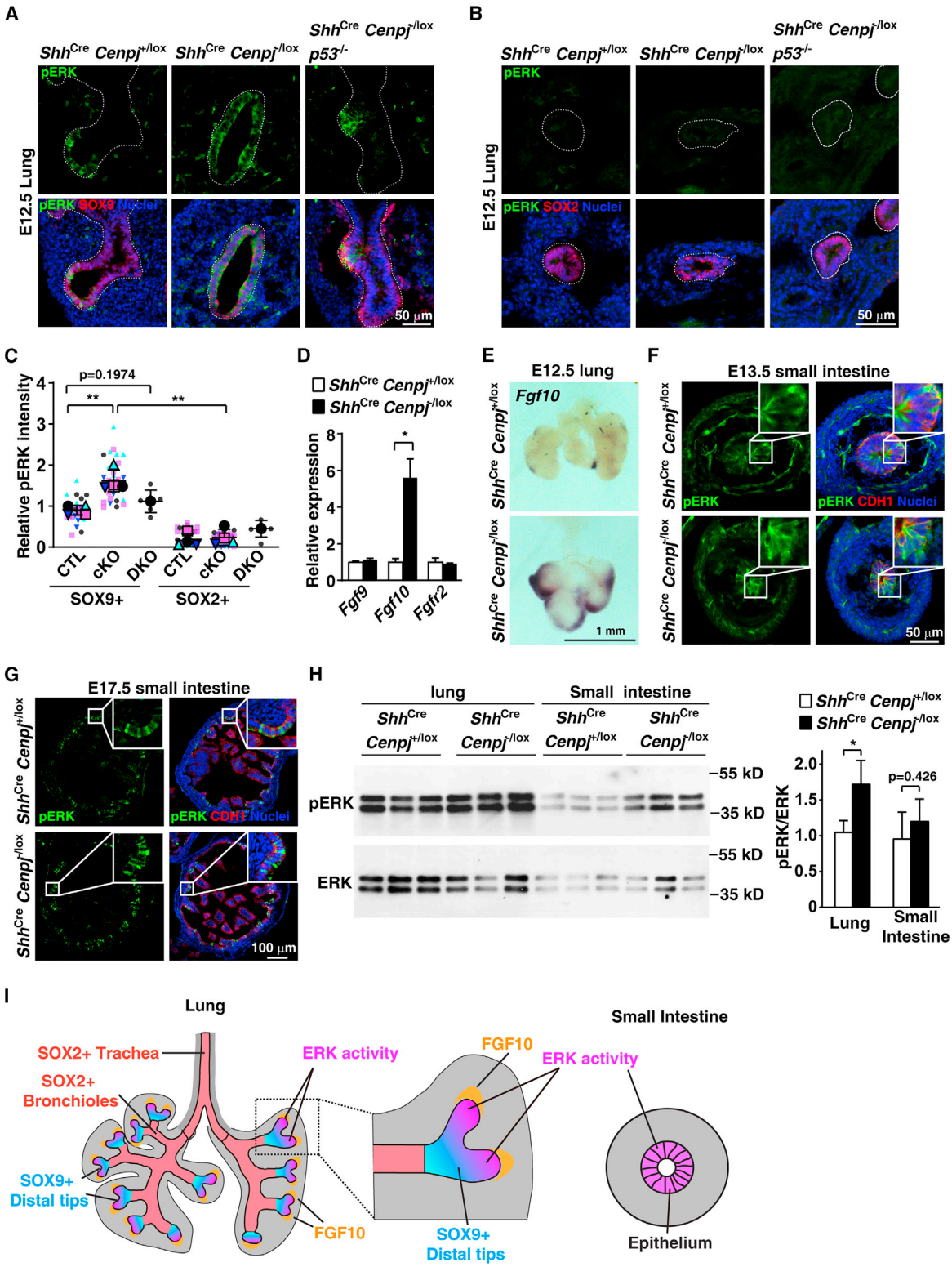

Figure 4. ERK activity correlates with survival of acentriolar cells

(A–C) Immunostaining (A and B) and quantification (C) of phospho-ERK (pERK) in E12.5 control (Shh^{Cre} $Cenpj^{+/lox}$), *Cenpj* loss-of-function (Shh^{Cre} $Cenpj^{-/lox}$), and *Cenpj* and *p53* combined loss-of-function (DKO, Shh^{Cre} $Cenpj^{-/lox}$ $p53^{-/-}$) lung sections. pERK was costained with SOX9 (A) or SOX2 (B), respectively. Scale bars, 50 μm. Data from 4 independent experiments for control and *Cenpj* loss of function were analyzed in the super plot; n = 6 for Shh^{Cre} $Cenpj^{-/lox}$ $p53^{-/-}$ from one experiment.

(legend continued on next page)

In the lung, ERK activity is restricted distally, whereas in the intestine, it is widespread

The loss of SOX2-expressing epithelial cells with the concomitant expansion of SOX9-expressing epithelial cells in acentriolar lungs suggested that some factors conferred tolerance to loss of centrioles in the SOX9-expressing progenitors at the distal developing lung buds. The signaling factor FGF10 is present specifically at the distal developing lung buds where it maintains the progenitor pool and drives bud growth (Arman et al., 1999; Bellusci et al., 1997; Min et al., 1998; Sekine et al., 1999; Volckaert et al., 2013). FGF signaling phosphorylates and activates ERK at the distal lung buds (Liu et al., 2004). Like FGF10, ERK's function in the lung epithelium is critical for lung development (Boucherat et al., 2014). Therefore, we investigated the possibility that ERK protects acentriolar cells from p53-mediated apoptosis.

As expected, phosphorylated ERK (pERK) was present in the distal tips of developing control lung buds overlapping with the SOX9-expressing progenitors (Figures 4A and 4C). pERK was not detected in the SOX2-expressing airway epithelium of control lungs (Figures 4B and 4C). In contrast, pERK was distributed throughout the epithelium of *Shh*^{Cre} *Cenpj*$^{-/lox}$ lungs (Figures 4A and 4C). Immunoblot for pERK confirmed that E13.5 *Shh*^{Cre} *Cenpj*$^{-/lox}$ lungs possess increased ERK activity (Figure 4H). Thus, ERK is active in surviving acentriolar cells, and in *Shh*^{Cre} *Cenpj*$^{-/lox}$ lungs, corresponding with the expansion of SOX9-expressing progenitors and the loss of SOX2-expressing epithelial cells.

In *Shh*^{Cre} *Cenpj*$^{-/lox}$ p53$^{-/-}$ lungs, pERK distribution pattern is restored to that of control lungs (Figures 4A and 4C). Thus, removing p53 both restores SOX2-expressing cells to acentriolar lungs and restores pERK-negative cells, consistent with the role for ERK activity in protecting against p53-mediated apoptosis.

Interestingly, *Fgf10* expression was also expanded in *Shh*^{Cre} *Cenpj*$^{-/lox}$ lungs and restricted to the distal lung buds of control lungs (Figures 4D and 4E). Thus, the preferential survival of *Fgf10*-expressing distal lung cells may account for the expansion of pERK in *Shh*^{Cre} *Cenpj*$^{-/lox}$ lungs.

Unlike the lungs, both control and *Shh*^{Cre} *Cenpj*$^{-/lox}$ intestinal epithelia displayed broad pERK distribution at both E13.5 and E17.5 (Figures 4F and 4G). Therefore, unlike the developing lungs where ERK activity is spatially restricted, ERK activity is widespread in the epithelium during intestinal development. Also unlike the case for the lung, immunoblot for pERK revealed no difference in ERK activity in E13.5 *Shh*^{Cre} *Cenpj*$^{-/lox}$ intestines (Figure 4H). The distribution of ERK activity in both developing lung and small intestine is schematized in Figure 4I, highlighting that ERK activity is restricted to the distal buds in the lungs and widespread in the developing intestine and raising the possibility that increased pERK underlies the selective survival of acentriolar cells.

ERK suppresses p53-dependent apoptosis in acentriolar lung progenitors

To test whether different ERK activity levels explain the different responses to loss of centrioles, we used SCH772984, a well-characterized and highly selective ERK antagonist (Chaikuad et al., 2014; Morris et al., 2013). Consistent with its ability to inhibit ERK, SCH772984 dramatically inhibited the growth and branching of epithelia of cultured lungs (Figures 5A–5C). In contrast, other kinase inhibitors, such as p38 MAPK inhibitor BIRB 796 (Pargellis et al., 2002) or JNK inhibitor JNK-IN-8 (Zhang et al., 2012), did not block the growth of cultured lungs (Figures 5A–5C). Thus, pharmacological inhibitors of ERK, like genetic inactivation (Boucherat et al., 2015b), disrupt lung branching. Although branching is already compromised in *Shh*^{Cre} *Cenpj*$^{-/lox}$ lungs, the addition of SCH772984 inhibited their growth, similar to control lungs (Figures 5A–5C), further suggesting that acentriolar cells depend on ERK activity.

To more quantitatively assess whether ERK activity sustains acentriolar lung and intestinal epithelial cells, we generated lung and intestinal epithelial organoids. More specifically, we generated *Shh*^{Cre} *Cenpj*$^{+/lox}$ *Rosa26*^{tdTomato} *Sox9*^{GFP} (control) and *Shh*^{Cre} *Cenpj*$^{-/lox}$ *Rosa26*^{tdTomato} *Sox9*^{GFP} (mutant) embryos that selectively express tdTomato throughout the endoderm. Progenitors from isolated lungs of both E12.5 control and mutants (Nichane et al., 2017) grew into sphere-shaped organoids (Figures 5D and S5A). SCH772984 reduced the growth of both control and acentriolar organoids (Figures 5D, S5A, S5B, S5D, S5E, S5F, S5G, S5H, and S5I). In addition to reducing organoid size, SC772984 blocked the ability of acentriolar progenitors to grow into sphere-like structures (Figure 5D). We also observed the reduction of Sox9-IRES-GFP expression in acentriolar organoids and SCH772984-treated control organoids, indicating the role of ERK activity in maintaining the expression of progenitor markers (Figures 5D, S5A, and S5C). Inhibiting ERK with SCH772984 did not affect apoptosis in control lung organoids (Figures 5E and 5F). However, in acentriolar lung organoids, SCH772984 dramatically activated apoptosis throughout the epithelium (Figures 5E and 5F). Thus, ERK activity is essential for lung progenitors to survive without centrioles.

We returned to consider the mystery of why CENPJ is critical for lung development but dispensable for intestinal development and hypothesized that widespread ERK activity protects acentriolar intestinal cells. To test whether ERK protects acentriolar intestinal cells from apoptosis, we generated intestinal epithelial organoids from E13.5 *Shh*^{Cre} *Cenpj*$^{+/lox}$ *Rosa26*^{tdTomato} and *Shh*^{Cre} *Cenpj*$^{-/lox}$ *Rosa26*^{tdTomato} embryos by culturing the epithelial progenitors in Matrigel (Andersson-Rolf et al., 2014). As with lung organoids, inhibiting ERK with SCH772984 did not affect apoptosis in control intestinal organoids (Figures 5G and 5H). And again, as with lung organoids, SCH772984 induced

(D) qRT-PCR measurement of *Fgf9*, *Fgf10*, and *Fgfr2* expression in E13.5 control (*Shh*^{Cre} *Cenpj*$^{+/lox}$) and *Cenpj* loss-of-function (*Shh*^{Cre} *Cenpj*$^{-/lox}$) lungs. *Fgf10* was upregulated. Data from 3 independent experiments were analyzed in super plot.

(E) *In situ* hybridization of *Fgf10* in E12.5 control (*Shh*^{Cre} *Cenpj*$^{+/lox}$) and *Cenpj* loss-of-function (*Shh*^{Cre} *Cenpj*$^{-/lox}$) lungs. Scale bars, 1 mm.

(F and G) Immunostaining of phospho-ERK (pERK) in E13.5 (F) and E17.5 (G) control (*Shh*^{Cre} *Cenpj*$^{+/lox}$) and *Cenpj* loss-of-function (*Shh*^{Cre} *Cenpj*$^{-/lox}$) small intestine sections. Inlets depicted magnified view of epithelium. Scale bars denote 50 and 100 μm, respectively.

(H) Immunoblots of phospho-ERK (pERK) and total ERK (ERK) in control (*Shh*^{Cre} *Cenpj*$^{+/lox}$) and *Cenpj* loss-of-function (*Shh*^{Cre} *Cenpj*$^{-/lox}$) lung and small intestine at E13.5. We quantified the ratio of pERK:ERK densitometry. n = 3.

(I) A schematic showing the distribution of ERK activity (magenta) in developing lungs and intestine.

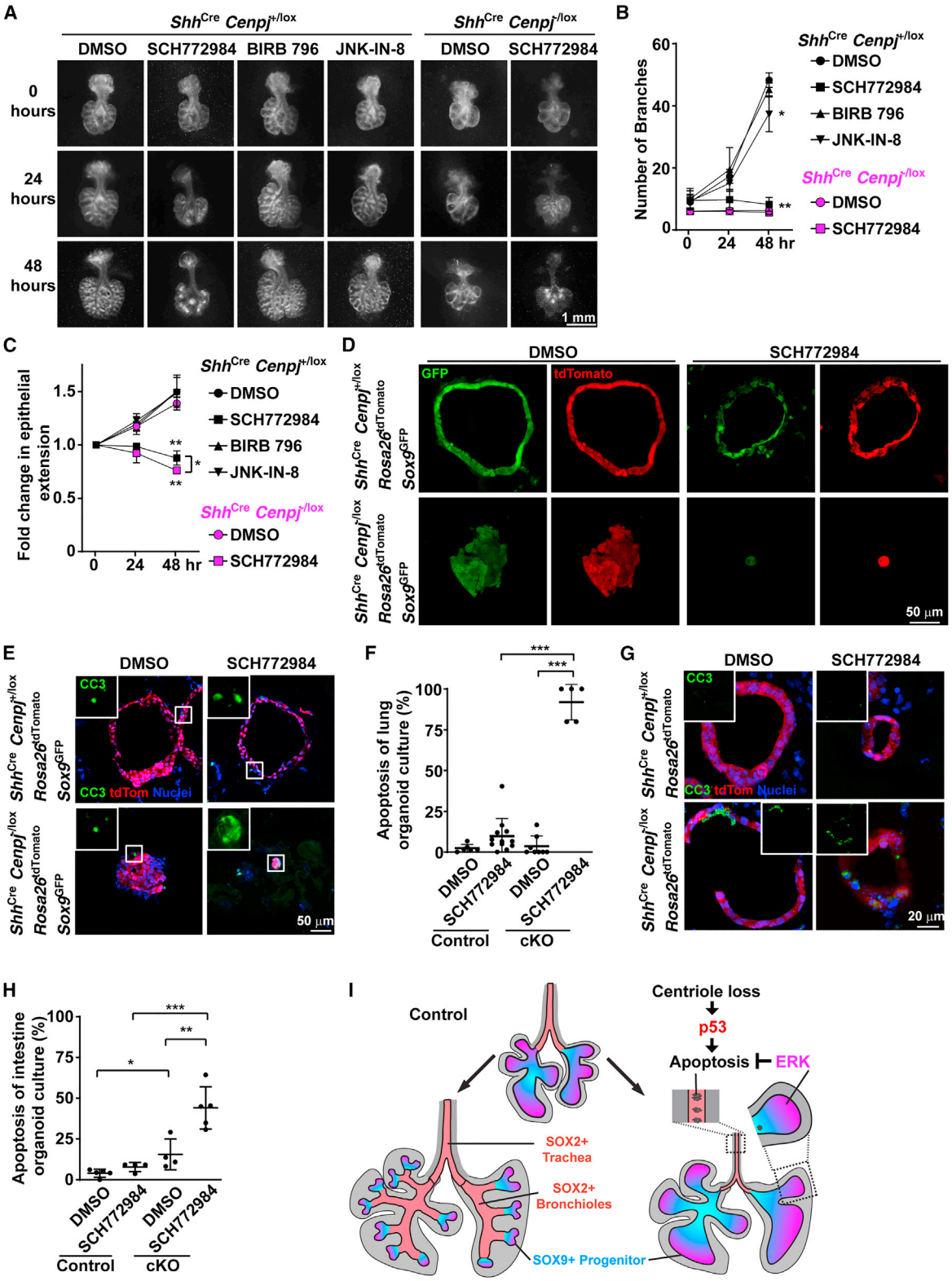

Figure 5. ERK activity protects acentriolar cells from p53-dependent apoptosis

(A) Control (*Shh*^{Cre} *Cenpj*$^{+/lox}$) and *Cenpj* loss-of-function (*Shh*^{Cre} *Cenpj*$^{-/lox}$) lungs were isolated at E11.5 and cultured on a semi-permeable membrane. Control lungs were treated with DMSO, SCH772984, BIRB 796, or JNK-IN-8 for 48 h. *Cenpj* loss-of-function lungs were treated with DMSO or SCH772984 for 48 h. Images were taken every 24 h. Scale bar, 1 mm.

(legend continued on next page)

apoptosis specifically in acentriolar intestinal organoids (Figures 5G and 5H). The growth of control and acentriolar intestinal organoids was similar to that of lung organoids with and without SCH772984 treatment (Figures S5C and S5D). These results demonstrate that ERK activity protects both intestinal and lung epithelium from apoptosis in the absence of centrioles.

Loss of centrioles activates p53 throughout the lung (Figures 3D and 3F), whereas ERK is activated specifically in the distal lung, suggesting that ERK activity does not affect the levels of p53. ERK activation is similar in control and Shh^{Cre} $Cenpj^{-/lox}$ $p53^{-/-}$ lungs (Figure 4A), indicating that p53 does not directly affect ERK activity. Therefore, we propose that ERK and p53 act in parallel, with loss of centrioles inducing p53 activation and cell death specifically when ERK activity is low (Figure 5I). Thus, in the endoderm, the developmental consequences of centriole loss and p53 activation are shaped by ERK. In the presence of ERK activation, as in SOX9-expressing lung epithelium and intestinal epithelium, cells tolerate loss of centrioles and p53 activation. However, without ERK activity, as in SOX2-expressing lung epithelium, loss of centrioles activates p53 to induce apoptosis.

DISCUSSION

Centrioles are essential for the proliferation of many animal cells *in vitro* and *in vivo* (Bazzi and Anderson, 2014; Doxsey et al., 2005; Faisst et al., 2002; Hudson et al., 2001; Izraeli et al., 1999; Rieder et al., 2001; Stevens et al., 2009; Tang et al., 2011; Wong et al., 2015). For example, centrioles are critical for early divisions in both *C. elegans* and *Drosophila* development (Rodrigues-Martins et al., 2008; Schwarz et al., 2018; Stevens et al., 2007). However, not all cell division requires centrioles. For example, the earliest divisions of mouse development occur without centrioles (Bangs et al., 2015; Dumont and Desai, 2012), later *Drosophila* divisions do not depend on centrioles (Basto et al., 2006), planaria cells divide without centrioles (Azimzadeh et al., 2012), and plants do not have centrioles (Brown and Lemmon, 2011).

Previous work shows the absence of centrioles causes cell death in rapidly proliferating mammalian lineages (Bazzi and Anderson, 2014). Therefore, we examined the function of the roles of centrioles in the endoderm, focusing on the lung and small intestine epithelium, two rapidly proliferating endodermal lineages (Miller et al., 1999). To our surprise, genetically removing centrioles from the endoderm had profound effects on one lineage (lung) but not another (intestine). Loss of centrioles in the lung epithelium blocked all branching after the formation of the major divisions, whereas the equivalent perturbation did not disrupt intestinal development.

Upon investigating why centrioles are differentially required for lung and intestine development, we discovered that, while loss of centrioles activated p53 in both, the phenotypic consequences of p53 activation were distinct. Indeed, even within the lung, activated p53 disrupted the formation of SOX2-expressing airway cells, but not of SOX9-expressing progenitors.

SOX2-expressing cells differentiate from SOX9-expressing progenitors and are present more proximal to the progenitors in the developing trachea, bronchi, and bronchioles. While we demonstrated that SOX2 itself is dispensable for lung branching, we propose that the SOX2-expressing cells themselves are critical to bifurcate the progenitor populations and create individualized buds. Consistent with this proposal, other mutations that decrease the number of SOX2-expressing cells also cause branching defects, although less profoundly than that caused by loss of CENPJ (Boucherat et al., 2015a; Li et al., 2018; Lin et al., 2017; Mahoney et al., 2014). Therefore, we propose that, in acentriolar lungs, the loss of SOX2-expressing cells prevents division of the progenitor pool, and the main lung divisions develop as large SOX9-expressing cysts. Perhaps the decreased ERK activity in SOX2-expressing cells causes branching by altering growth at branchpoints.

Removing p53 dramatically rescued the development of acentriolar lungs, even restoring viability. In contrast, limb development was not restored by removing p53 and the limb patterning defect was recapitulated by removing cilia, indicating that cilia are essential for limb development independent of p53 activity. Moreover, removing cilia in the endoderm did not affect lung morphogenesis. Together, these results confirm that centrioles are essential for cilium-mediated signaling but that cilia and ciliary signaling are not critical for lung patterning. In brain development, removing p53 only partially rescued phenotypes caused by loss of centrioles (Lin et al., 2020). In contrast, the critical function of centrioles in lung morphogenesis is to restrain p53 activity.

Activation of p53 has different developmental consequences in different tissues (Bowen et al., 2019). The factors that dictate

(B and C) We measured the number of branches (B) and epithelial extension (C) of the lungs from (A). The fold change of epithelial extension was normalized to that immediately before the addition of the indicated compounds (i.e., at 0 h). DMSO treatment was compared with BIRB 796, JNK-IN-8, or SCH772984 treatment within the same genotype using unpaired t test. n = 3.

(D) Visualization of GFP and tdTomato fluorescence in control (Shh^{Cre} $Cenpj^{+/lox}$ $R26^{tdTomato}$ $Sox9^{GFP}$) and *Cenpj* loss-of-function (Shh^{Cre} $Cenpj^{-/lox}$ $R26^{tdTomato}$ $Sox9^{GFP}$) lung organoid culture cryosections. Scale bar, 50 μm. Note: parameters of GFP fluorescence were adjusted in each group for better visualization.

(E and F) Staining (E) and quantification (F) of cleaved Casp3 (CC3) in control (Shh^{Cre} $Cenpj^{+/lox}$ $R26^{tdTomato}$ $Sox9^{GFP}$) and *Cenpj* loss-of-function (Shh^{Cre} $Cenpj^{-/lox}$ $R26^{tdTomato}$ $Sox9^{GFP}$) lung organoid culture cryosections. Inlets show the magnified view of cleaved Casp3 staining. Scale bar, 50 μm. DMSO treatment was compared with SCH772984 treatment within the same genotype, and a different genotype with the same treatment was compared using unpaired t test. n = 6, 12, 8, and 5, respectively.

(G and H) Staining (G) and quantification (H) of Cleaved Casp3 (CC3) stained in control (Shh^{Cre} $Cenpj^{+/lox}$ $R26^{tdTomato}$) and *Cenpj* loss-of-function (Shh^{Cre} $Cenpj^{-/lox}$ $R26^{tdTomato}$) intestinal organoid culture cryosections. Inlets show cleaved Casp3 staining. Scale bar, 20 μm. DMSO treatment was compared with SCH772984 treatment within the same genotype, and a different genotype with the same treatment was compared using unpaired t test. n = 5, 4, 4, and 5, respectively.

(I) A schematic illustrating the differential responses of lung epithelial cells to loss of centrioles. Loss of centrioles induced p53 activation in the endodermal epithelium. Acentriolar lung cells with low ERK activity (SOX2-expressing cells) apoptose, whereas acentriolar lung SOX9-expressing progenitors with higher ERK activity survive and grow.

See also Figure S5.

this differential impact are not understood but could include differences in timing of activation, differences in degree of activation, or differences in transcriptional context. Removing MDM2 caused a transient upregulation of p53 during early lung development in part of the epithelium and modestly increased apoptosis, disrupted separation of the esophagus and trachea, and delayed but did not block branching and differentiation of the airway epithelium (Bowen et al., 2019; Sui et al., 2019). In contrast, we found that p53 activation caused by loss of centrioles blocked branching and the differentiation of lung SOX9+ progenitors into SOX2+ bronchiolar cells. We surmise that loss of centrioles activates p53 to a greater extent than loss of MDM2.

As we observed that SOX9-expressing cells are relatively resistant to p53-mediated apoptosis in acentriolar lungs, we also considered whether their position at the distal bud tips may be relevant. FGF10 is expressed specifically at the distal lung buds where it activates ERK (Arman et al., 1999; Bellusci et al., 1997; Liu et al., 2004; Min et al., 1998; Sekine et al., 1999; Volckaert et al., 2013). We found that ERK was specifically active in a subset of the SOX9-expressing progenitors, raising the possibility that ERK activation shapes the response to p53 activation. Consistent with that possibility, pharmacologically inhibiting ERK induced apoptosis specifically in acentriolar SOX9-expressing cells. Unlike the lungs, ERK activity in the intestine is widely distributed, but in this tissue too, inhibiting ERK specifically induced apoptosis in acentriolar cells. Therefore, we propose that the spatial distribution of ERK activity shapes the outcome of loss of centrioles. We predict that ERK activity will also shape the phenotypic outcomes of other cell stresses that activate p53 and may explain the differential impacts of centriolar abnormalities and p53 activation outside the endoderm. For example, centrioles and ERK activity are both important for brain growth (Basson et al., 2008; Bazzi and Anderson, 2014; Meyers et al., 1998; Pucilowska et al., 2012; Raballo et al., 2000; Shi et al., 2014). Perhaps one reason microcephaly, associated with centriolar defects, affects cerebral growth more than the midbrain is that FGF8 protects midbrain cells from apoptosis.

Mutation of p53 is an extremely common hallmark of diverse cancers, particularly lung cancers, many of which express SOX2 (Gibbons et al., 2014; Karachaliou et al., 2013). Centriolar abnormalities are also common in cancer cells (Marteil et al., 2018). Our finding that, during development, SOX2-expressing lung cells apoptose without CENPJ but are rescued by loss of p53 is consistent with the possibility that, in tumor suppression, p53 removes cells with centriolar abnormalities. Of course, activated ERK is another hallmark of diverse cancers, including some lung cancers (Feldser et al., 2010; Junttila et al., 2010; Vicent et al., 2004). One prediction of this work on noncancerous tissues is that cancers that retain wild-type p53, like hepatocellular carcinoma, will either have unaltered centrioles or will possess oncogenic mutations that activate ERK. Our work further suggests that ERK activity inhibition could be particularly efficacious in cancers with retained p53 activity.

Our work reveals that centrioles are differentially required by different lineages during endoderm development, and spatial distribution of ERK activity shapes the phenotypic outcomes of centriole-loss-induced p53 activation.

Limitations of study

The role of ERK activity in shaping the acentriolar output is revealed by the correlation of ERK activity distribution and survival pattern and tested by chemically inhibiting ERK in lung and intestinal organoid cultures that have high ERK activity. Confirming that high ERK activity can protect SOX2+-expressing airway cells from apoptosis *in vivo* will require activating ERK activity in the proximal acentriolar lung.

STAR★METHODS

Detailed methods are provided in the online version of this paper and include the following:

- KEY RESOURCES TABLE
- RESOURCE AVAILABILITY
  - Lead contact
  - Materials availability
  - Data and code availability
- EXPERIMENTAL MODEL AND SUBJECT DETAILS
  - Mice
- METHOD DETAILS
  - Lung and intestinal culture
  - Immunostaining
  - Wholemount lung staining
  - Next-generation RNA sequencing and analysis
  - Quantitative real-time PCR
  - Immunoblotting
- QUANTIFICATION AND STATISTICAL ANALYSIS

SUPPLEMENTAL INFORMATION

Supplemental information can be found online at https://doi.org/10.1016/j.devcel.2021.11.020.

ACKNOWLEDGMENTS

We are grateful to Ace Lewis and Jeffrey Bush at UCSF for generating *Sox2* conditional knockout embryos. We thank David Erle, Andrea Barczak, Matthew Aber, and Joshua Rudolph at the UCSF Functional Genomics Core Facility and Lauren Byrnes for help with RNA-seq and analysis. We thank E Yu for husbandry and genotyping of the mice used in this study. We thank Ross J. Metzger, Francisco Hernan Espinoza, and Mark A. Krasnow at Stanford University, Nan Tang at the National Institute of Biological Sciences, Beijing, and Gail R. Martin at UCSF for thoughtful discussions. We also thank the members of the Reiter lab for critical comments and suggestions on the study. This work was funded by NIH R01GM095941, R01AR054396, and R01HD089918 to J.F.R. and GVA PROMETEO/2019/075 to J.M.G.V.

AUTHOR CONTRIBUTIONS

C.X. conceived and executed most experiments. S.R.A. generated Figure 1E. V.H.P. and J.M.G.V. generated electron microscopy images in Figures 1C, 1D, S1, and S2. C.X. and J.F.R. wrote the manuscript. J.F.R. supervised the study.

DECLARATION OF INTERESTS

The authors declare no competing interests.

Received: February 23, 2021
Revised: September 5, 2021
Accepted: November 17, 2021
Published: December 20, 2021

REFERENCES

Abdelhamed, Z.A., Natarajan, S., Wheway, G., Inglehearn, C.F., Toomes, C., Johnson, C.A., and Jagger, D.J. (2015). The Meckel-Gruber syndrome protein TMEM67 controls basal body positioning and epithelial branching morphogenesis in mice via the non-canonical Wnt pathway. Dis. Model. Mech. *8*, 527–541. https://doi.org/10.1242/dmm.019083.

Afgan, E., Baker, D., Batut, B., van den Beek, M., Bouvier, D., Cech, M., Chilton, J., Clements, D., Coraor, N., Grüning, B.A., et al. (2018). The Galaxy platform for accessible, reproducible and collaborative biomedical analyses: 2018 update. Nucleic Acids Res. *46*, W537–W544. https://doi.org/10.1093/nar/gky379.

Ahn, S., and Joyner, A.L. (2004). Dynamic changes in the response of cells to positive hedgehog signaling during mouse limb patterning. Cell *118*, 505–516. https://doi.org/10.1016/j.cell.2004.07.023.

Alanis, D.M., Chang, D.R., Akiyama, H., Krasnow, M.A., and Chen, J. (2014). Two nested developmental waves demarcate a compartment boundary in the mouse lung. Nat. Commun. *5*, 3923. https://doi.org/10.1038/ncomms4923.

Al-Dosari, M.S., Shaheen, R., Colak, D., and Alkuraya, F.S. (2010). Novel CENPJ mutation causes Seckel syndrome. J. Med. Genet. *47*, 411–414. https://doi.org/10.1136/jmg.2009.076646.

Allen, M.A., Andrysik, Z., Dengler, V.L., Mellert, H.S., Guarnieri, A., Freeman, J.A., Sullivan, K.D., Galbraith, M.D., Luo, X., Kraus, W.L., et al. (2014). Global analysis of p53-regulated transcription identifies its direct targets and unexpected regulatory mechanisms. eLife *3*, e02200. https://doi.org/10.7554/eLife.02200.

Andersson-Rolf, A., Fink, J., Mustata, R.C., and Koo, B.K. (2014). A video protocol of retroviral infection in primary intestinal organoid culture. J. Vis. Exp. *90*, e51765. https://doi.org/10.3791/51765.

Arman, E., Haffner-Krausz, R., Gorivodsky, M., and Lonai, P. (1999). FGFR2 is required for limb outgrowth and lung-branching morphogenesis. Proc. Natl. Acad. Sci. USA *96*, 11895–11899. https://doi.org/10.1073/pnas.96.21.11895.

Aubrey, B.J., Kelly, G.L., Janic, A., Herold, M.J., and Strasser, A. (2018). How does p53 induce apoptosis and how does this relate to p53-mediated tumour suppression? Cell Death Differ. *25*, 104–113. https://doi.org/10.1038/cdd.2017.169.

Azimzadeh, J., Wong, M.L., Downhour, D.M., Sánchez Alvarado, A., and Marshall, W.F. (2012). Centrosome loss in the evolution of planarians. Science *335*, 461–463. https://doi.org/10.1126/science.1214457.

Bangs, F.K., Schrode, N., Hadjantonakis, A.K., and Anderson, K.V. (2015). Lineage specificity of primary cilia in the mouse embryo. Nat. Cell Biol. *17*, 113–122. https://doi.org/10.1038/ncb3091.

Basson, M.A., Echevarria, D., Ahn, C.P., Sudarov, A., Joyner, A.L., Mason, I.J., Martinez, S., and Martin, G.R. (2008). Specific regions within the embryonic midbrain and cerebellum require different levels of FGF signaling during development. Development *135*, 889–898. https://doi.org/10.1242/dev.011569.

Basto, R., Lau, J., Vinogradova, T., Gardiol, A., Woods, C.G., Khodjakov, A., and Raff, J.W. (2006). Flies without centrioles. Cell *125*, 1375–1386. https://doi.org/10.1016/j.cell.2006.05.025.

Bazzi, H., and Anderson, K.V. (2014). Acentriolar mitosis activates a p53-dependent apoptosis pathway in the mouse embryo. Proc. Natl. Acad. Sci. USA *111*, E1491–E1500. https://doi.org/10.1073/pnas.1400568111.

Beers, M.F., Wali, A., Eckenhoff, M.F., Feinstein, S.I., Fisher, J.H., and Fisher, A.B. (1992). An antibody with specificity for surfactant protein C precursors: identification of pro-SP-C in rat lung. Am. J. Respir. Cell Mol. Biol. *7*, 368–378. https://doi.org/10.1165/ajrcmb/7.4.368.

Bellusci, S., Grindley, J., Emoto, H., Itoh, N., and Hogan, B.L. (1997). Fibroblast growth factor 10 (FGF10) and branching morphogenesis in the embryonic mouse lung. Development *124*, 4867–4878.

Bond, J., Roberts, E., Springell, K., Lizarraga, S.B., Scott, S., Higgins, J., Hampshire, D.J., Morrison, E.E., Leal, G.F., Silva, E.O., et al. (2005). A centrosomal mechanism involving CDK5RAP2 and CENPJ controls brain size. Nat. Genet. *37*, 353–355. https://doi.org/10.1038/ng1539.

Boucherat, O., Landry-Truchon, K., Bérubé-Simard, F.A., Houde, N., Beuret, L., Lezmi, G., Foulkes, W.D., Delacourt, C., Charron, J., and Jeannotte, L. (2015a). Epithelial inactivation of Yy1 abrogates lung branching morphogenesis. Development *142*, 2981–2995. https://doi.org/10.1242/dev.120469.

Boucherat, O., Nadeau, V., Bérubé-Simard, F.A., Charron, J., and Jeannotte, L. (2014). Crucial requirement of ERK/MAPK signaling in respiratory tract development. Development *141*, 3197–3211. https://doi.org/10.1242/dev.110254.

Boucherat, O., Nadeau, V., Bérubé-Simard, F.A., Charron, J., and Jeannotte, L. (2015b). Crucial requirement of ERK/MAPK signaling in respiratory tract development. Development *142*, 3801. https://doi.org/10.1242/dev.131821.

Bowen, M.E., and Attardi, L.D. (2019). The role of p53 in developmental syndromes. J. Mol. Cell Biol. *11*, 200–211. https://doi.org/10.1093/jmcb/mjy087.

Bowen, M.E., McClendon, J., Long, H.K., Sorayya, A., Van Nostrand, J.L., Wysocka, J., and Attardi, L.D. (2019). The spatiotemporal pattern and intensity of p53 activation dictates phenotypic diversity in p53-driven developmental syndromes. Dev. Cell *50*, 212–228.e6. https://doi.org/10.1016/j.devcel.2019.05.015.

Brosh, R., Sarig, R., Natan, E.B., Molchadsky, A., Madar, S., Bornstein, C., Buganim, Y., Shapira, T., Goldfinger, N., Paus, R., and Rotter, V. (2010). p53-dependent transcriptional regulation of EDA2R and its involvement in chemotherapy-induced hair loss. FEBS Lett. *584*, 2473–2477. https://doi.org/10.1016/j.febslet.2010.04.058.

Brown, R.C., and Lemmon, B.E. (2011). Dividing without centrioles: innovative plant microtubule organizing centres organize mitotic spindles in bryophytes, the earliest extant lineages of land plants. AoB Plants *2011*, plr028. https://doi.org/10.1093/aobpla/plr028.

Carraro, G., del Moral, P.M., and Warburton, D. (2010). Mouse embryonic lung culture, a system to evaluate the molecular mechanisms of branching. J. Vis. Exp. *40*, 2035.

Chaikuad, A., Tacconi, E.M., Zimmer, J., Liang, Y., Gray, N.S., Tarsounas, M., and Knapp, S. (2014). A unique inhibitor binding site in ERK1/2 is associated with slow binding kinetics. Nat. Chem. Biol. *10*, 853–860. https://doi.org/10.1038/nchembio.1629.

Chan, H.Y., Sivakamasundari, V., Xing, X., Kraus, P., Yap, S.P., Ng, P., Lim, S.L., and Lufkin, T. (2011). Comparison of IRES and F2A-based locus-specific multicistronic expression in stable mouse lines. PLoS One *6*, e28885. https://doi.org/10.1371/journal.pone.0028885.

Davenport, J.R., Watts, A.J., Roper, V.C., Croyle, M.J., van Groen, T., Wyss, J.M., Nagy, T.R., Kesterson, R.A., and Yoder, B.K. (2007). Disruption of intraflagellar transport in adult mice leads to obesity and slow-onset cystic kidney disease. Curr. Biol. *17*, 1586–1594. https://doi.org/10.1016/j.cub.2007.08.034.

Doxsey, S., McCollum, D., and Theurkauf, W. (2005). Centrosomes in cellular regulation. Annu. Rev. Cell Dev. Biol. *21*, 411–434. https://doi.org/10.1146/annurev.cellbio.21.122303.120418.

Dumont, J., and Desai, A. (2012). Acentrosomal spindle assembly and chromosome segregation during oocyte meiosis. Trends Cell Biol. *22*, 241–249. https://doi.org/10.1016/j.tcb.2012.02.007.

Dyson, J.M., Conduit, S.E., Feeney, S.J., Hakim, S., DiTommaso, T., Fulcher, A.J., Sriratana, A., Ramm, G., Horan, K.A., Gurung, R., et al. (2017). INPP5E regulates phosphoinositide-dependent cilia transition zone function. J. Cell Biol. *216*, 247–263. https://doi.org/10.1083/jcb.201511055.

el-Deiry, W.S., Tokino, T., Velculescu, V.E., Levy, D.B., Parsons, R., Trent, J.M., Lin, D., Mercer, W.E., Kinzler, K.W., and Vogelstein, B. (1993). WAF1, a potential mediator of p53 tumor suppression. Cell *75*, 817–825. https://doi.org/10.1016/0092-8674(93)90500-p.

Faisst, A.M., Alvarez-Bolado, G., Treichel, D., and Gruss, P. (2002). Rotatin is a novel gene required for axial rotation and left-right specification in mouse embryos. Mech. Dev. *113*, 15–28. https://doi.org/10.1016/s0925-4773(02)00003-5.

Feldser, D.M., Kostova, K.K., Winslow, M.M., Taylor, S.E., Cashman, C., Whittaker, C.A., Sanchez-Rivera, F.J., Resnick, R., Bronson, R., Hemann, M.T., and Jacks, T. (2010). Stage-specific sensitivity to p53 restoration during

lung cancer progression. Nature *468*, 572–575. https://doi.org/10.1038/nature09535.

Forsberg, K., Wuttke, A., Quadrato, G., Chumakov, P.M., Wizenmann, A., and Di Giovanni, S. (2013). The tumor suppressor p53 fine-tunes reactive oxygen species levels and neurogenesis via PI3 kinase signaling. J. Neurosci. *33*, 14318–14330. https://doi.org/10.1523/JNEUROSCI.1056-13.2013.

Gibbons, D.L., Byers, L.A., and Kurie, J.M. (2014). Smoking, p53 mutation, and lung cancer. Mol. Cancer Res. *12*, 3–13. https://doi.org/10.1158/1541-7786.MCR-13-0539.

Gönczy, P. (2012). Towards a molecular architecture of centriole assembly. Nat. Rev. Mol. Cell Biol. *13*, 425–435. https://doi.org/10.1038/nrm3373.

Harfe, B.D., Scherz, P.J., Nissim, S., Tian, H., McMahon, A.P., and Tabin, C.J. (2004). Evidence for an expansion-based temporal Shh gradient in specifying vertebrate digit identities. Cell *118*, 517–528. https://doi.org/10.1016/j.cell.2004.07.024.

Harper, J.W., Adami, G.R., Wei, N., Keyomarsi, K., and Elledge, S.J. (1993). The p21 Cdk-interacting protein Cip1 is a potent inhibitor of G1 cyclin-dependent kinases. Cell *75*, 805–816. https://doi.org/10.1016/0092-8674(93)90499-g.

Huangfu, D., and Anderson, K.V. (2005). Cilia and Hedgehog responsiveness in the mouse. Proc. Natl. Acad. Sci. USA *102*, 11325–11330. https://doi.org/10.1073/pnas.0505328102.

Hudson, J.W., Kozarova, A., Cheung, P., Macmillan, J.C., Swallow, C.J., Cross, J.C., and Dennis, J.W. (2001). Late mitotic failure in mice lacking Sak, a polo-like kinase. Curr. Biol. *11*, 441–446. https://doi.org/10.1016/s0960-9822(01)00117-8.

Izraeli, S., Lowe, L.A., Bertness, V.L., Good, D.J., Dorward, D.W., Kirsch, I.R., and Kuehn, M.R. (1999). The SIL gene is required for mouse embryonic axial development and left-right specification. Nature *399*, 691–694. https://doi.org/10.1038/21429.

Jacks, T., Remington, L., Williams, B.O., Schmitt, E.M., Halachmi, S., Bronson, R.T., and Weinberg, R.A. (1994). Tumor spectrum analysis in p53-mutant mice. Curr. Biol. *4*, 1–7. https://doi.org/10.1016/s0960-9822(00)00002-6.

Junttila, M.R., Karnezis, A.N., Garcia, D., Madriles, F., Kortlever, R.M., Rostker, F., Brown Swigart, L., Pham, D.M., Seo, Y., Evan, G.I., and Martins, C.P. (2010). Selective activation of p53-mediated tumour suppression in high-grade tumours. Nature *468*, 567–571. https://doi.org/10.1038/nature09526.

Karachaliou, N., Rosell, R., and Viteri, S. (2013). The role of SOX2 in small cell lung cancer, lung adenocarcinoma and squamous cell carcinoma of the lung. Transl. Lung Cancer Res. *2*, 172–179. https://doi.org/10.3978/j.issn.2218-6751.2013.01.01.

Kastenhuber, E.R., and Lowe, S.W. (2017). Putting p53 in context. Cell *170*, 1062–1078. https://doi.org/10.1016/j.cell.2017.08.028.

Kopinke, D., Roberson, E.C., and Reiter, J.F. (2017). Ciliary hedgehog signaling restricts injury-induced adipogenesis. Cell *170*, 340–351.e12. https://doi.org/10.1016/j.cell.2017.06.035.

Lazzaro, D., Price, M., de Felice, M., and Di Lauro, R. (1991). The transcription factor TTF-1 is expressed at the onset of thyroid and lung morphogenesis and in restricted regions of the foetal brain. Development *113*, 1093–1104.

Lessel, D., Wu, D., Trujillo, C., Ramezani, T., Lessel, I., Alwasiyah, M.K., Saha, B., Hisama, F.M., Rading, K., Goebel, I., et al. (2017). Dysfunction of the MDM2/p53 axis is linked to premature aging. J. Clin. Invest. *127*, 3598–3608. https://doi.org/10.1172/JCI92171.

Li, Q., Jiao, J., Li, H., Wan, H., Zheng, C., Cai, J., and Bao, S. (2018). Histone arginine methylation by Prmt5 is required for lung branching morphogenesis through repression of BMP signaling. J. Cell Sci. *131*, jcs217406. https://doi.org/10.1242/jcs.217406.

Lin, C., Yao, E., Zhang, K., Jiang, X., Croll, S., Thompson-Peer, K., and Chuang, P.T. (2017). YAP is essential for mechanical force production and epithelial cell proliferation during lung branching morphogenesis. eLife *6*, e21130. https://doi.org/10.7554/eLife.21130.

Lin, Y.N., Lee, Y.S., Li, S.K., and Tang, T.K. (2020). Loss of CPAP in developing mouse brain and its functional implication for human primary microcephaly. J. Cell Sci. *133*, jcs243592. https://doi.org/10.1242/jcs.243592.

Liu, Y., Stein, E., Oliver, T., Li, Y., Brunken, W.J., Koch, M., Tessier-Lavigne, M., and Hogan, B.L. (2004). Novel role for Netrins in regulating epithelial behavior during lung branching morphogenesis. Curr. Biol. *14*, 897–905. https://doi.org/10.1016/j.cub.2004.05.020.

Madisen, L., Zwingman, T.A., Sunkin, S.M., Oh, S.W., Zariwala, H.A., Gu, H., Ng, L.L., Palmiter, R.D., Hawrylycz, M.J., Jones, A.R., et al. (2010). A robust and high-throughput Cre reporting and characterization system for the whole mouse brain. Nat. Neurosci. *13*, 133–140. https://doi.org/10.1038/nn.2467.

Mahoney, J.E., Mori, M., Szymaniak, A.D., Varelas, X., and Cardoso, W.V. (2014). The hippo pathway effector Yap controls patterning and differentiation of airway epithelial progenitors. Dev. Cell *30*, 137–150. https://doi.org/10.1016/j.devcel.2014.06.003.

Marino, S., Vooijs, M., van Der Gulden, H., Jonkers, J., and Berns, A. (2000). Induction of medulloblastomas in p53-null mutant mice by somatic inactivation of Rb in the external granular layer cells of the cerebellum. Genes Dev. *14*, 994–1004.

Marshall, C.B., Mays, D.J., Beeler, J.S., Rosenbluth, J.M., Boyd, K.L., Santos Guasch, G.L., Shaver, T.M., Tang, L.J., Liu, Q., Shyr, Y., et al. (2016). p73 is required for multiciliogenesis and regulates the Foxj1-associated gene network. Cell Rep. *14*, 2289–2300. https://doi.org/10.1016/j.celrep.2016.02.035.

Marteil, G., Guerrero, A., Vieira, A.F., de Almeida, B.P., Machado, P., Mendonça, S., Mesquita, M., Villarreal, B., Fonseca, I., Francia, M.E., et al. (2018). Over-elongation of centrioles in cancer promotes centriole amplification and chromosome missegregation. Nat. Commun. *9*, 1258. https://doi.org/10.1038/s41467-018-03641-x.

McQuin, C., Goodman, A., Chernyshev, V., Kamentsky, L., Cimini, B.A., Karhohs, K.W., Doan, M., Ding, L., Rafelski, S.M., Thirstrup, D., et al. (2018). CellProfiler 3.0: next-generation image processing for biology. PLoS Biol. *16*, e2005970. https://doi.org/10.1371/journal.pbio.2005970.

Metzger, R.J., Klein, O.D., Martin, G.R., and Krasnow, M.A. (2008). The branching programme of mouse lung development. Nature *453*, 745–750. https://doi.org/10.1038/nature07005.

Meyers, E.N., Lewandoski, M., and Martin, G.R. (1998). An FGF8 mutant allelic series generated by Cre- and Flp-mediated recombination. Nat. Genet. *18*, 136–141. https://doi.org/10.1038/ng0298-136.

Miller, S.A., Adornato, M., Briglin, A., Cavanaugh, M., Christian, T., Jewett, K., Michaelson, C., Monoson, T., Price, F., Tignor, J., and Tyrell, D. (1999). Domains of differential cell proliferation suggest hinged folding in avian gut endoderm. Dev. Dyn. *216*, 398–410. https://doi.org/10.1002/(SICI)1097-0177(199912)216:4/5<398::AID-DVDY8>3.0.CO;2-7.

Min, H., Danilenko, D.M., Scully, S.A., Bolon, B., Ring, B.D., Tarpley, J.E., DeRose, M., and Simonet, W.S. (1998). Fgf-10 is required for both limb and lung development and exhibits striking functional similarity to Drosophila branchless. Genes Dev. *12*, 3156–3161. https://doi.org/10.1101/gad.12.20.3156.

Morris, E.J., Jha, S., Restaino, C.R., Dayananth, P., Zhu, H., Cooper, A., Carr, D., Deng, Y., Jin, W., Black, S., et al. (2013). Discovery of a novel ERK inhibitor with activity in models of acquired resistance to BRAF and MEK inhibitors. Cancer Discov. *3*, 742–750. https://doi.org/10.1158/2159-8290.CD-13-0070.

Nemajerova, A., Kramer, D., Siller, S.S., Herr, C., Shomroni, O., Pena, T., Gallinas Suazo, C., Glaser, K., Wildung, M., Steffen, H., et al. (2016). TAp73 is a central transcriptional regulator of airway multiciliogenesis. Genes Dev. *30*, 1300–1312. https://doi.org/10.1101/gad.279836.116.

Nichane, M., Javed, A., Sivakamasundari, V., Ganesan, M., Ang, L.T., Kraus, P., Lufkin, T., Loh, K.M., and Lim, B. (2017). Isolation and 3D expansion of multipotent Sox9+ mouse lung progenitors. Nat. Methods *14*, 1205–1212. https://doi.org/10.1038/nmeth.4498.

Pargellis, C., Tong, L., Churchill, L., Cirillo, P.F., Gilmore, T., Graham, A.G., Grob, P.M., Hickey, E.R., Moss, N., Pav, S., and Regan, J. (2002). Inhibition of p38 MAP kinase by utilizing a novel allosteric binding site. Nat. Struct. Biol. *9*, 268–272. https://doi.org/10.1038/nsb770.

Pucilowska, J., Puzerey, P.A., Karlo, J.C., Galán, R.F., and Landreth, G.E. (2012). Disrupted ERK signaling during cortical development leads to abnormal progenitor proliferation, neuronal and network excitability and

behavior, modeling human neuro-cardio-facial-cutaneous and related syndromes. J. Neurosci. *32*, 8663–8677. https://doi.org/10.1523/JNEUROSCI.1107-12.2012.

Que, J., Okubo, T., Goldenring, J.R., Nam, K.T., Kurotani, R., Morrisey, E.E., Taranova, O., Pevny, L.H., and Hogan, B.L. (2007). Multiple dose-dependent roles for Sox2 in the patterning and differentiation of anterior foregut endoderm. Development *134*, 2521–2531. https://doi.org/10.1242/dev.003855.

Raballo, R., Rhee, J., Lyn-Cook, R., Leckman, J.F., Schwartz, M.L., and Vaccarino, F.M. (2000). Basic fibroblast growth factor (FGF2) is necessary for cell proliferation and neurogenesis in the developing cerebral cortex. J. Neurosci. *20*, 5012–5023.

Rawlins, E.L., Clark, C.P., Xue, Y., and Hogan, B.L. (2009). The Id2+ distal tip lung epithelium contains individual multipotent embryonic progenitor cells. Development *136*, 3741–3745. https://doi.org/10.1242/dev.037317.

Rieder, C.L., Faruki, S., and Khodjakov, A. (2001). The centrosome in vertebrates: more than a microtubule-organizing center. Trends Cell Biol. *11*, 413–419. https://doi.org/10.1016/s0962-8924(01)02085-2.

Rodrigues-Martins, A., Riparbelli, M., Callaini, G., Glover, D.M., and Bettencourt-Dias, M. (2008). From centriole biogenesis to cellular function: centrioles are essential for cell division at critical developmental stages. Cell Cycle *7*, 11–16. https://doi.org/10.4161/cc.7.1.5226.

Schindelin, J., Arganda-Carreras, I., Frise, E., Kaynig, V., Longair, M., Pietzsch, T., Preibisch, S., Rueden, C., Saalfeld, S., Schmid, B., et al. (2012). Fiji: an open-source platform for biological-image analysis. Nat. Methods *9*, 676–682. https://doi.org/10.1038/nmeth.2019.

Schwarz, A., Sankaralingam, P., O'Connell, K.F., and Müller-Reichert, T. (2018). Revisiting centrioles in nematodes-historic findings and current topics. Cells *7*, 101. https://doi.org/10.3390/cells7080101.

Sekine, K., Ohuchi, H., Fujiwara, M., Yamasaki, M., Yoshizawa, T., Sato, T., Yagishita, N., Matsui, D., Koga, Y., Itoh, N., and Kato, S. (1999). FGF10 is essential for limb and lung formation. Nat. Genet. *21*, 138–141.

Shaham, O., Smith, A.N., Robinson, M.L., Taketo, M.M., Lang, R.A., and Ashery-Padan, R. (2009). Pax6 is essential for lens fiber cell differentiation. Development *136*, 2567–2578. https://doi.org/10.1242/dev.032888.

Shi, L., Lin, Q., and Su, B. (2014). Human-specific hypomethylation of CENPJ, a key brain size regulator. Mol. Biol. Evol. *31*, 594–604. https://doi.org/10.1093/molbev/mst231.

Stevens, N.R., Dobbelaere, J., Wainman, A., Gergely, F., and Raff, J.W. (2009). Ana3 is a conserved protein required for the structural integrity of centrioles and basal bodies. J. Cell Biol. *187*, 355–363. https://doi.org/10.1083/jcb.200905031.

Stevens, N.R., Raposo, A.A., Basto, R., St Johnston, D., and Raff, J.W. (2007). From stem cell to embryo without centrioles. Curr. Biol. *17*, 1498–1503. https://doi.org/10.1016/j.cub.2007.07.060.

Sui, P., Li, R., Zhang, Y., Tan, C., Garg, A., Verheyden, J.M., and Sun, X. (2019). E3 ubiquitin ligase MDM2 acts through p53 to control respiratory progenitor cell number and lung size. Development *146*, dev179820. https://doi.org/10.1242/dev.179820.

Tang, C.J., Lin, S.Y., Hsu, W.B., Lin, Y.N., Wu, C.T., Lin, Y.C., Chang, C.W., Wu, K.S., and Tang, T.K. (2011). The human microcephaly protein STIL interacts with CPAP and is required for procentriole formation. EMBO J. *30*, 4790–4804. https://doi.org/10.1038/emboj.2011.378.

Toki, T., Yoshida, K., Wang, R., Nakamura, S., Maekawa, T., Goi, K., Katoh, M.C., Mizuno, S., Sugiyama, F., Kanezaki, R., et al. (2018). De novo mutations activating germline TP53 in an inherited bone-marrow-failure syndrome. Am. J. Hum. Genet. *103*, 440–447. https://doi.org/10.1016/j.ajhg.2018.07.020.

Turrell, F.K., Kerr, E.M., Gao, M., Thorpe, H., Doherty, G.J., Cridge, J., Shorthouse, D., Speed, A., Samarajiwa, S., Hall, B.A., et al. (2017). Lung tumors with distinct p53 mutations respond similarly to p53 targeted therapy but exhibit genotype-specific statin sensitivity. Genes Dev. *31*, 1339–1353. https://doi.org/10.1101/gad.298463.117.

Van Nostrand, J.L., Brady, C.A., Jung, H., Fuentes, D.R., Kozak, M.M., Johnson, T.M., Lin, C.Y., Lin, C.J., Swiderski, D.L., Vogel, H., et al. (2014). Inappropriate p53 activation during development induces features of CHARGE syndrome. Nature *514*, 228–232. https://doi.org/10.1038/nature13585.

Vicent, S., López-Picazo, J.M., Toledo, G., Lozano, M.D., Torre, W., Garcia-Corchón, C., Quero, C., Soria, J.C., Martín-Algarra, S., Manzano, R.G., and Montuenga, L.M. (2004). ERK1/2 is activated in non-small-cell lung cancer and associated with advanced tumours. Br. J. Cancer *90*, 1047–1052. https://doi.org/10.1038/sj.bjc.6601644.

Volckaert, T., Campbell, A., Dill, E., Li, C., Minoo, P., and De Langhe, S. (2013). Localized FGF10 expression is not required for lung branching morphogenesis but prevents differentiation of epithelial progenitors. Development *140*, 3731–3742. https://doi.org/10.1242/dev.096560.

Wong, Y.L., Anzola, J.V., Davis, R.L., Yoon, M., Motamedi, A., Kroll, A., Seo, C.P., Hsia, J.E., Kim, S.K., Mitchell, J.W., et al. (2015). Cell biology. Reversible centriole depletion with an inhibitor of Polo-like kinase 4. Science *348*, 1155–1160. https://doi.org/10.1126/science.aaa5111.

Yang, H.W., Chung, M., Kudo, T., and Meyer, T. (2017). Competing memories of mitogen and p53 signalling control cell-cycle entry. Nature *549*, 404–408. https://doi.org/10.1038/nature23880.

Zhang, T., Inesta-Vaquera, F., Niepel, M., Zhang, J., Ficarro, S.B., Machleidt, T., Xie, T., Marto, J.A., Kim, N., Sim, T., et al. (2012). Discovery of potent and selective covalent inhibitors of JNK. Chem. Biol. *19*, 140–154. https://doi.org/10.1016/j.chembiol.2011.11.010.

Zhu, K., Wang, J., Zhu, J., Jiang, J., Shou, J., and Chen, X. (1999). p53 induces TAP1 and enhances the transport of MHC class I peptides. Oncogene *18*, 7740–7747. https://doi.org/10.1038/sj.onc.1203235.

Zorn, A.M., and Wells, J.M. (2009). Vertebrate endoderm development and organ formation. Annu. Rev. Cell Dev. Biol. *25*, 221–251. https://doi.org/10.1146/annurev.cellbio.042308.113344.

STAR★METHODS

KEY RESOURCES TABLE

REAGENT or RESOURCE	SOURCE	IDENTIFIER
Antibodies		
Anti-FGFR1OP (FOP, Rabbit)	Proteintech	Cat#11343-1-AP, PRID: AB_2103362
Anti-ARL13B (Rabbit)	Proteintech	Cat#17711-1-AP, PRID: AB_2060867
Anti-CDH1 (Rat)	Invitrogen	Cat#13-1900, PRID: AB_2533005
Anti-γTubulin (Goat)	Santa Cruz	Cat#sc-7396, PRID: AB_2211262
Anti-p53 (Rabbit)	Proteintech	Cat#10442-1-AP, PRID: AB_2206609
Anti-p21 (Rabbit)	Proteintech	Cat#28248-1-AP, PRID: AB_2881097
Anti-Cleaved Caspase-3 (Rabbit)	Cell Signaling Technology	Cat#9661S, PRID: AB_2341188 9664S
Anti-SOX2 (Rabbit)	Cell Signaling Technology	Cat#23064S, PRID: AB_2714146
Anti-SOX2 (Goat)	R&D	Cat#AF2018, PRID: AB_355110
Anti-SOX9 (Goat)	R&D	Cat#AF3075, PRID: AB_2194160
Anti-TTF-1 (Nkx2.1, Rabbit)	Cell Signaling Technology	Cat#12373S, PRID: AB_2797895
Anti-Prosurfactant Protein C (SFTPC, Rabbit)	Sigma	Cat#AB3786, PRID: AB_91588
Anti-p73 (Rabbit)	Abcam	Cat#ab40658, PRID: AB_776999
Anti-Phospho-p44/42 MAPK (pErk1/2, Rabbit)	Cell Signaling Technology	Cat#9101S, PRID: AB_331646
Anti-Phospho-p44/42 MAPK (pErk1/2, Rabbit)	Cell Signaling Technology	Cat#4370S, PRID: AB_2315112
Anti-p44/42 MAPK (Erk1/2, Rabbit)	Cell Signaling Technology	Cat#4695S, PRID: AB_390779
Anti-Ki67 (Rabbit)	Abcam	Cat#ab15580, RRID: AB_443209
Donkey anti-rat Alexa Fluor 488	Invitrogen	Cat#A-21208, PRID: AB_2535794
Donkey anti-goat Alexa Fluor 647	Invitrogen	Cat#A-21447, PRID: AB_2535864
Donkey anti-rabbit Alexa Fluor 568	Invitrogen	Cat#A-10042, PRID: AB_2534017
Goat Anti-Rabbit IgG HRP.	Jackson ImmunoResearch	Cat#111-035-144, PRID: AB_2307391
Anti-Cdh1 e660	eBioscience	Cat#50-3249-82, PRID: AB_11040003
Anti-Pecam1/CD31 e450	eBioscience	Cat#480311, PRID: AB_10598807
Anti-Ptprc/CD45 e450	eBioscience	Cat#480451, PRID: AB_1518807
Anti-Ter119 e450	eBioscience	Cat#485921, PRID: AB_1518809
Bacterial and virus strains		
Stable Competent *E. coli*	NEB	Cat#C3040H
Chemicals, peptides, and recombinant proteins		
SCH772984	MedChemExpress	Cat#HY-50846
Doramapimod (BIRB 796)	MedChemExpress	Cat#HY-10320
JNK-IN-8	MedChemExpress	Cat#HY-13319
FluorSave	E.M.D. Millipore Calbiochem	Cat#34-578-920ML
Hoechst 33342	Thermo Fisher	Cat#H21492
EdU	Thermo Fisher	Cat#E10187
PhosSTOP	Roche	Cat#04906845001
cOmplete™ EDTA-free Protease Inhibitor Cocktail	Roche	Cat#11873580001
Phenol red-free Leibovitz L-15	Thermo Fisher	Cat#21083027
Advanced DMEM/F12	Thermo Fisher	Cat#12634010
Collagenase I	Thermo Fisher	Cat#17100017

(*Continued on next page*)

Continued

REAGENT or RESOURCE	SOURCE	IDENTIFIER
Collagenase II	Thermo Fisher	Cat#17101015
Dnase I	Thermo Fisher	Cat#04716728001
Trypsin	Thermo Fisher	Cat#27250018
FBS	Gibco	Cat#10439-024
BSA	Sigma	Cat#A9418
HEPES	Thermo Fisher	Cat#15630080
EDTA	Thermo Fisher	Cat#15575020
RNasin Ribonuclease Inhibitor	Promega	Cat#N2115
Growth Factor Reduced, Phenol Red-Free Matrigel 10 mg/mL	Corning	Cat#356231
Fgf10	R&D	Cat#6224-FG-025
Fgf9	R&D	Cat#7399-F9-025
EGF	R&D	Cat#2028-EG-200
CHIR99021	Tocris	Cat#4423
Y27632	Tocris	Cat#1254
A8301	Tocris	Cat#2939
Heparin	Sigma	Cat#H3149
Insulin	Roche	Cat#11376497001
Transferrin	Roche	Cat#10652202001
PenStrep	Thermo Fisher	Cat#15140122
Glutamine	Thermo Fisher	Cat#25030081
Anti-Anti	Thermo Fisher	Cat#15240062
Dispase II	Thermo Fisher	Cat#17105041
Collagenase IV	Thermo Fisher	Cat#17104019
Papain	Worthington	Cat#LS003118
Noggin	Peprotech	Cat#10772-456
R-Spondin 1	R&D	Cat#7150-RS-025/CF
TRI reagent	Sigma	Cat#T9424
SuperSignal™ West Pico PLUS Chemiluminescent Substrate	Thermo Fisher	Cat#PI34577
SuperSignal™ West Femto Maximum Sensitivity Substrate	Thermo Fisher	Cat#34095
Critical commercial assays		
PowerUp™ SYBRTM Green Master Mix	Applied Biosystems	Cat#A25742
iScript cDNA synthesis kit	BioRad	Cat#1708890
RNeasy Mini Kit (250)	Qiagen	Cat#74106
Zymo RNA Clean & Concentrator-5 columns	Zymo Research	Cat#1016
Deposited data		
Raw and processed RNAseq data	This paper	GEO: GSE188585
Raw Western blot images	This paper	Mendeley Data: https://doi.org/10.17632/tdwstr46bb.1
Experimental models: Organisms/strains		
Mouse: C57BL/6J	The Jackson Laboratory	Jax stock 000664
Mouse: *Shh*^{Cre}: B6.Cg-*Shh*$^{tm1(E.G.F.P./cre)Cjt}$/J	The Jackson Laboratory	Jax stock 005622
Mouse: *Ift88*^{l}ox: B6.129P2-*Ift88*^{tm1Bky}/J	The Jackson Laboratory	Jax stock 022409
Mouse: *Sox2*^{lox}:*Sox2*$^{tm1.1Lan}$/J	The Jackson Laboratory	Jax stock 013093
Mouse: *R26*^{tdTomato}: *Rosa26*$^{tm14(CAG-tdTomato)Hze/J}$	The Jackson Laboratory	Jax stock 007914

(*Continued on next page*)

Continued

REAGENT or RESOURCE	SOURCE	IDENTIFIER
Mouse: *Sox9*^{GFP}:*Sox9*$^{IRES-EGFP}$	The Jackson Laboratory	Jax stock 030137
Mouse ES cell: *Cenpj*$^{tm1a(EUCOMM.)Wtsi}$	European Mouse Mutant Cell Repository	EPD0028_7_G05
Mouse: p53 KO: B6.129S2-*Trp53*$^{tm1Tyj/J}$	The Jackson Laboratory	Jax stock 002101
Mouse: p53^{LoxP}: B6.129P2-*Trp53*$^{tm1Brn/J}$	The Jackson Laboratory	Jax stock 008462
Mouse: *ACTB:FLPe*: B6;SJL-Tg(ACTFLPe) 9205Dym/J	The Jackson Laboratory	Jax stock 005703
Mouse: β-actin-cre: B6N.FVB-Tmem163Tg(ACTB-cre)2Mrt/CjDswJ	The Jackson Laboratory	Jax stock 019099
Oligonucleotides		
qPCR-Fgf9-F: GGAGTTGGATATA CCTCGCCT	This paper	N/A
qPCR-Fgf9-R: TGATCCATACAG CTCCCCCT	This paper	N/A
qPCR-Fgf10-F: GGAGATGTCCG CTGGAGAAG	This paper	N/A
qPCR-Fgf10-R: GCTGTTGATGG CTTTGACGG	This paper	N/A
qPCR-Fgfr2-F: TTTCCTCCGAGA TCATCGCC	This paper	N/A
qPCR-Fgfr2-R: ACCATGGGCTA CCTGCAATG	This paper	N/A
qPCR-TAp63-F: ATTCAGTTGGA GCAAGGGGG	This paper	N/A
qPCR-TAp63-R: CACGAGAAATG AGCTGGGGT	This paper	N/A
qPCR-DNp63-F: CAGCCTTGACC AGTCTCACT	This paper	N/A
qPCR-DNp63-R: TGTCTTCGCAA TCTGGCAGT	This paper	N/A
qPCR-Dolk-F: CAGTGTGGGAC CGATACTCCT	(Kopinke et al., 2017)	N/A
qPCR-Dolk-R: CCAAGCAAAG GCATGACCA	(Kopinke et al., 2017)	N/A
qPCR-Hprt-F: CATAACCTGGTT CATCATCGC	(Kopinke et al., 2017)	N/A
qPCR-Hprt-R: TCCTCCTCAG ACCGCTTTT	(Kopinke et al., 2017)	N/A
qPCR-Pde12-F: ACCTTTTGGG TGCCAGTAGA	(Kopinke et al., 2017)	N/A
qPCR-Pde12-R: CCAGAGGTC ATCTGTCCTTCA	(Kopinke et al., 2017)	N/A
Software and algorithms		
SDS. Software version 2.3	Thermo Fisher	https://www.thermofisher.com/us/en/home/technical-resources/software-downloads/applied-biosystems-7500-real-time-pcr-system.html
QuantStudio™ Design & Analysis 1.3.1	Thermo Fisher	https://www.thermofisher.com/us/en/home/global/forms/life-science/quantstudio-3-5-software.html
Prism 8 for Windows	GraphPad Software	www.graphpad.com
CellProfiler version 3.1.9	(McQuin et al., 2018)	https://cellprofiler.org/releases/
R Studio	Rstudio	https://rstudio.com/products/rstudio/download/

(*Continued on next page*)

Continued

REAGENT or RESOURCE	SOURCE	IDENTIFIER
R	The R Foundation	https://cran.r-project.org/mirrors.html
Galaxy	(Afgan et al., 2018)	https://usegalaxy.org/
FIJI	(Schindelin et al., 2012)	https://imagej.net/Fiji
Zen version 3.1 blue edition	Zeiss	https://www.zeiss.com/microscopy/us/products/microscope-software/zen.html

RESOURCE AVAILABILITY

Lead contact

Requests for further information or reagents can be directed to and will be fulfilled by the Lead Contact, Jeremy Reiter (Jeremy.Reiter@ucsf.edu), Department of Biochemistry and Biophysics, Cardiovascular Research Institute, University of California, San Francisco.

Materials availability

The Cenpj$^{+/-}$ and *Cenpj*$^{lox/lox}$ mice generated in this study will be made available upon request. We may require a completed materials transfer agreement and reasonable compensation by the requestor for its processing and shipping.

Data and code availability

RNA-seq data have been deposited at GEO and are publicly available as of the date of publication. Accession numbers are listed in the key resources table. Original immunoblot images have been deposited at Mendeley and are publicly available as of the date of publication. The DOI is listed in the key resources table. Microscopy data reported in this paper will be shared by the lead contact upon request.

This manuscript did not generate new code.

Any additional information required to reanalyze the data reported in this paper is available from the lead contact upon request.

EXPERIMENTAL MODEL AND SUBJECT DETAILS

Mice

Shh^{Cre} [*Shh*$^{tm1(E.G.F.P./Cre)Cjt}$], *Ift88*^{lox} (*Ift88*^{tm1Bky}), *Sox2*^{lox} (*Sox2*$^{tm1.1Lan}$), *R26*^{tdTomato} [*Rosa26*$^{tm14(CAG-tdTomato)Hze/J}$], *Sox9*^{GFP} (*Sox9*$^{IRES-EGFP}$), p53 KO (B6.129S2-*Trp53*$^{tm1Tyj/J}$), and p53^{LoxP} (B6.129P2-*Trp53*$^{tm1Brn/J}$) alleles have been described previously (Chan et al., 2011; Davenport et al., 2007; Harfe et al., 2004; Jacks et al., 1994; Madisen et al., 2010; Marino et al., 2000; Shaham et al., 2009). The knockout first *Cenpj*$^{tm1a(EUCOMM.)Wtsi}$ ES cells were purchased from the European Mutant Mice Repository. The conditional allele (*Cenpj*^{lox}) was generated by crossing *Cenpj*$^{tm1a(EUCOMM.)Wtsi}$ mice to *Actb:FLPe* mice (JAX Stock No: 005703). The null allele (*Cenpj*$^{-}$) was generated by crossing the *Cenpj*$^{lox/+}$ mice to *β-actin-Cre* mice (JAX Stock No: 019099). C57BL/6J mice (JAX Stock No: 000664) were purchased from Jackson Laboratory. 6-24 week old male *Shh*^{Cre} *Cenpj*$^{+/-}$, or *Shh*^{Cre} *Cenpj*$^{+/-}$ *Sox9*$^{GFP/GFP}$, or *Shh*^{Cre} *Cenpj*$^{+/-}$ *p53*$^{+/-}$ mice were mated with 6-24 week old female *Cenpj*$^{lox/lox}$, or *Cenpj*$^{lox/lox}$ *Rosa26*$^{tdTomato/tdTomato}$, or *Cenpj*$^{lox/lox}$ *p53*$^{+/-}$, or *Cenpj*$^{lox/lox}$ *p53*$^{lox/lox}$ mice. 6-24 week old male *Shh*^{Cre} *Ift88*$^{+/-}$ mice were mated with 6-24 week old female *Ift88*$^{lox/lox}$ mice. 6-24 week old male *Shh*^{Cre} *Sox2*$^{+/lox}$ mice were mated with 6-24 week old female *Sox2*$^{lox/lox}$ mice. Embryos were collected in a sex-unbiased manner.

All mice were maintained under specific pathogen-free conditions at the UCSF animal care facility. Mice were cared for, and all experiments were approved by the Administrative Panel on Laboratory Care, and the Institutional Animal Care and Use Committee (IACUC) of UCSF Mice were maintained on a normal chow diet.

METHOD DETAILS

Lung and intestinal culture

Lung progenitors from E12.5 control (*Shh*^{Cre} *Cenpj*$^{+/lox}$ *R26*^{tdTomato} *Sox9*^{GFP} or *Shh*^{Cre} *Cenpj*$^{+/lox}$), *Cenpj* loss of function (*Shh*^{Cre} *Cenpj*$^{-/lox}$ *R26*^{tdTomato} *Sox9*^{GFP} or *Shh*^{Cre} *Cenpj*$^{-/lox}$), and *Cenpj* and *p53* combined loss of function (*Shh*^{Cre} *Cenpj*$^{-/lox}$ p53$^{-/-}$) embryos were isolated and cultured as described (Nichane et al., 2017). Briefly, lungs were digested with collagenase I and II, mixed with 10% FBS/DMEM and filtered and washed twice in DMEM/F12. GFP+ cells were collected or all the cells were collected and counted. About 1000 cells were seeded into 40 μl Matrigel in 24-well plate. Twenty minutes after Matrigel solidified, 500 μl culture medium was added. Twenty-four hours later, the organoid culture was incubated with DMSO or 2.5 μM SCH772984 for 24 hours and then imaged directly, or subjected to frozen section, immunostaining and imaged using a Zeiss LSM800 confocal laser scanning microscope.

Embryonic intestinal cells were isolated from E13.5 control (*Shh*^{Cre} *Cenpj*$^{+/lox}$ *R26*^{tdTomato}) and *Cenpj* loss of function (*Shh*^{Cre} *Cenpj*$^{-/lox}$ *R26*^{tdTomato}) embryos and cultured as described (Andersson-Rolf et al., 2014). Briefly, small intestine were cut longitudinally

and incubated with 2 mM EDTA for 30 min at 4°C and then digested in 1 ml Trypsin buffer at 37°C for 10 min. Then the samples were changed to 10%FBS/DMEM and pipetted up and down, then filtered. The cells were washed twice, then about 2000 cells were seeded into Matrigel. Twenty-four hours after the seeding in Matrigel, the intestinal culture was incubated with DMSO or 2.5 μM SCH772984 for 24 hours before being imaged for tdTomato fluorescence. Intestinal organoids isolated from control (*Shh*^{Cre} *Cenpj*$^{+/lox}$), *Cenpj* loss of function (*Shh*^{Cre} *Cenpj*$^{-/lox}$), and *Cenpj* and *p53* combined loss of function (*Shh*^{Cre} *Cenpj*$^{-/lox}$ p53$^{-/-}$) embryos were cultured and treated with DMSO or 2.5 μM SCH772984 for 24 hours, then subjected to frozen section and immunostaining.

Wholemount lungs isolated from E11.5 control (*Shh*^{Cre} *Cenpj*$^{+/lox}$) and *Cenpj* loss of function (*Shh*^{Cre} *Cenpj*$^{-/lox}$) embryos were isolated and cultured as described (Carraro et al., 2010). Briefly, lungs were dissected and isolated at E11.5. Then lungs were placed on the top of semi-permeable membrane in 24-well plate loaded with 10% FBS/DMEM. The concentrations of the chemical compounds were used as follows: ERK1/2 inhibitor SCH772984 at 2.5 μM, p38 MAPK inhibitor Doramapimod (BIRB 796) at 10 μM, JNK1/2/3 inhibitor JNK-IN-8 at 10 μM. Images were taken every 24 hours with Zeiss Discovery V12 stereomicroscope.

Immunostaining

Embryos were immediately fixed in 4% paraformaldehyde at 4°C after dissection. Lung tissue was isolated and further fixed in 4% paraformaldehyde at 4°C for 2 hours. After fixation, the tissue was washed three times with ice-cold PBS. Then samples were dehydrated in 30% sucrose at 4°C overnight before being embedded in OCT and stored at -80°C. 12 μm frozen sections were washed three times with PBS and incubated with primary antibodies diluted in IF buffer (5% donkey serum and 0.3% Triton X-100 in PBS) at 4°C overnight. Then slides were washed five times with IF buffer and incubated with fluorescent secondary antibodies and Hoechst 33342 at room temperature for 2 hours, followed by five washes with IF buffer. Slides were mounted with FluorSave. Confocal images were obtained with Zeiss LSM800 confocal laser scanning microscope.

For EdU labeling, 600 μl 2.5 mg/ml EdU/D.P.B.S. solution was intraperitoneally injected into pregnant female mice at E11.5. After 15 minutes, the injected females were euthanized, and the embryonic lungs were dissected and fixed in 4% paraformaldehyde at 4°C for 1 hour. Then the fixed lungs were washed with ice-cold PBS three times and embedded in OCT. Frozen sections were first stained with primary antibodies, fluorescent secondary antibodies. Then EdU staining was performed according to the manufacturer's protocol (C10269, Thermo Fisher Scientific). Slides were washed three times with PBS, and Hoechst was stained for 5 minutes before being mounted with FluorSave mounting medium.

Wholemount lung staining

Wholemount lung staining was carried out as described previously (Metzger et al., 2008). Briefly, samples were fixed in 4% paraformaldehyde for 1 hour. Then, samples were washed in PBS for 3 times and gradually dehydrated to pure methanol. After incubation in 5% H2O2 in methanol for 5 hours at room temperature, samples were subjected to blocking and permeabilization in 5% dankey serum/1% Triton/PBS, then incubated with primary antibodies overnight at 4°Cin blocking buffer, washed with blocking buffer for 5 times. Then samples were incubated with fluorescent secondary antibodies overnight at 4°C. Samples were washed and further fixed in 4% paraformaldehyde for 30 min at 4°C after the staining and then cleared according to the iDISCO protocol. Samples were stored in DBE and imaged with AZ100 wide field light-sheet microscope at Nikon Imaging Center at UCSF. Images were processed with Micro-Manager 2.0 gamma and Image J. Max projection of the z-stacks were presented.

Next-generation RNA sequencing and analysis

E11.5 lungs and intestines from control (*Shh*$^{Cre/+}$ *Cenpj*$^{+/lox}$), Cenpj loss of function (*Shh*$^{Cre/+}$ *Cenpj*$^{-/lox}$) and *Ift88* loss of function (*Shh*$^{Cre/+}$ *Ift88*$^{-/lox}$) embryos were isolated and homogenized in 1 ml Trizol, followed by mixing with 200 μl chloroform and centrifugation at 12,000 rpm at 4°C for 15 min. The aqueous phase was transferred to new tubes and mixed with an equal volume of pure ethanol. Then the samples were processed with the QIAGEN RNeasy Micro kit for RNA extraction, followed by library construction at UCSF Functional Genomics Core Facility. Paired-end 150 bp (PE150) sequencing data were generated on an Illumina NovaSeq 6000. Differential gene expression among Control, *Cenpj* loss of function, and *Ift88* loss of function lung and intestine were assessed. Differential gene expression was called significant if FDR (adjusted p-value) < 0.05.

The common list of differentially expressed genes between control (*Shh*$^{Cre/+}$ *Cenpj*$^{+/lox}$) and *Cenpj* loss of function (*Shh*$^{Cre/+}$ *Cenpj*$^{-/lox}$) lungs, and between *Cenpj* loss of function (*Shh*$^{Cre/+}$ *Cenpj*$^{-/lox}$) and *Ift88* loss of function (*Shh*$^{Cre/+}$ *Ift88*$^{-/lox}$) lungs were chosen for heatmap analysis if FDR <0.05 and FC (fold change) >1.5 or FC < 0.67. Gene expression was normalized to the control group.

Volcano plot was generated from the $\log_2$(FC) and FDR of gene expression calculated from *Cenpj* loss of function (*Shh*$^{Cre/+}$ *Cenpj*$^{-/lox}$) versus control (*Shh*$^{Cre/+}$ *Cenpj*$^{+/lox}$) lungs. Upregulated genes were highlighted in red if the FDR<0.0.5 and $\text{Log}_2(\text{FC}) \geq 1$ ($\text{FC} \geq 2$); downregulated genes were highlighted in blue if the FDR<0.0.5 and $\text{Log}_2(\text{FC}) \leq -1$ ($\text{FC} \leq 1/2$).

Quantitative real-time PCR

RNA was extracted using the Trizol and RNeasy Kit (QIAGEN), and cDNA was synthesized using BioRad iScript cDNA synthesis kit (BioRad, 1708890). Quantitative real-time PCR was performed using PowerUp™ SYBRTM Green Master Mix (Applied Biosystems, A25742) in TempPlate polypropylene 384-well PCR plates (USA Scientific, 1438-4700) on QuantStudio 5 qPCR machine. Expression levels were normalized to the geometric average expression of *Dolk, Hprt* and *Pde12*.

Immunoblotting

Lung and small intestine were isolated from E13.5 control (*Shh*$^{Cre/+}$ *Cenpj*$^{+/lox}$) and *Cenpj* loss of function (*Shh*$^{Cre/+}$ *Cenpj*$^{-/lox}$) embryos in ice-cold PBS. Then samples were lysed in RIPA buffer supplemented with sufficient protease inhibitor (Roche, cOmplete™ Protease Inhibitor Cocktail, #11697498001) and phosphatase inhibitor (Roche, PhosSTOP, #04906845001). The supernatant was mixed with 4X loading buffer and heated at 100°C for 10 minutes before being loaded onto PAGE gel for electrophoresis. Then proteins were transferred from PAGE gel to PVDF membrane and incubated with primary antibodies ERK (1:1000) and pERK (1:1000) at 4°C overnight. After five washes with TBST, HRP conjugated secondary antibodies were incubated at room temperature for 1 hour and washed five times in TBST before being developed for ECL imaging with BioRad ChemiDoc Imager. SuperSignal™ West Pico PLUS Chemiluminescent Substrate for ERK and SuperSignal™ West Femto Maximum Sensitivity Substrate for pERK were used in the ECL reaction.

QUANTIFICATION AND STATISTICAL ANALYSIS

Gut isolated from E16.5 control (*Shh*^{Cre} *Cenpj*$^{+/lox}$ *Rosa26*^{tdTomato}) and *Cenpj* loss of function (*Shh*^{Cre} *Cenpj*$^{-/lox}$ *Rosa26*^{tdTomato}) embryos were dissected and placed onto a petri dish. Tissue was linearized to the petri dish by gently removing PBS. Images were taken along with a ruler under the ZEISS Discovery V12 stereomicroscope. Then the length of the small intestine, as well as ruler, were measured using the segmented line tool of ImageJ. Pixel length was then transformed into millimeters.

The branches of cultured wholemount lungs from control (*Shh*^{Cre} *Cenpj*$^{+/lox}$) and *Cenpj* loss of function (*Shh*^{Cre} *Cenpj*$^{-/lox}$) embryos were counted based on the images taken every 24 hours. The distance between left and right edges of epithelium was measured with ImageJ. Each measurement was normalized to that of the lungs at 0 hours immediately before the incubation of indicated compounds.

Quantification of the immunostaining images was carried out in CellProfiler (version 3.1.9). First, primary objects of "Epithelium," "Nuclei," "SOX2" or "SOX9" were identified from images stained with CDH1, Hoechst, SOX2 or SOX9 respectively, with "Method to distinguish clumped objects" and "Method to draw dividing lines between clumped objects" set as "Intensity". Then RelateObjects was used to identify SOX2-expressing epithelium or SOX9-expressing epithelium by setting "Epithelium" as the Parent Objects and "SOX2" or "SOX9" as the Child Objects. The newly identified objects were the nuclei of cells positive in SOX2 (nuclear) and CDH1, or SOX9 (nuclear) and CDH1. Mean intensity of p53 and p21 was measured in the objects of SOX2-expressing epithelium or SOX9-expressing epithelium. The average mean intensity was calculated and used for statistics.

For cleaved Caspase3 and phospho-ERK quantification, RelateObjects was used to identify SOX2-expressing epithelium or SOX9-expressing epithelium by setting "Epithelium" as the "Child Objects". The related objects were outlined by "Epithelium" (CDH1) and included the whole cells. Mean intensity of phospho-ERK, the number of cleaved Caspase3-positive cells were measured in these objects. The average mean intensity was calculated and used for statistics.

For wholemount staining of cleaved Caspase 3 quantification, SOX2+ epithelium (trachea & bronchi) were manually outlined. The mean intensity of cleaved Caspase 3 was measured by Image J.

For EdU quantification, primary objects "EdU labeled" were identified from EdU staining channel. Objects of "Epithelial nuclei" were identified with MaskObjects by masking primary objects "Epithelium" from primary objects "Nuclei". Then EdU labeled epithelial nuclei were identified with RelateObjects by setting "Epithelial Nuclei" as the Child Objects and "EdU labeled" as the Parent Objects. Then EdU positive nuclei were counted against the total nuclei in "Epithelium".

For the size of organoid cultures, the primary objects were identified from tdTomato fluorescence with "Method to distinguish clumped objects" and "Method to draw dividing lines between clumped objects" set as "Shape" so that objects were whole sphere-shaped organoids. MajorAxisLength was measured for each sphere-shaped organoid.

Then, the counted number or the averaged mean intensity from each image were calculated and used as one dot in the plots. Super plots were generated from 3-4 independent experiments with the average of each experiment as one datum. Data were represented as the mean±standard deviation. One-way ANOVA analysis was performed to check whether the data were significant. Then p-value between every two groups was determined using unpaired two-tailed t-tests for single plots or paired two-tailed t-tests for super plots. Unless otherwise stated, statistical analyses were performed in GraphPad Prism. A p-value less than 0.05 was considered statistically significant and denoted as follows: *<0.05, **<0.01, ***<0.001.